Physics of Fluids

Annular Poiseuille flow of Bingham fluids with wall slip

Cite as: Phys. Fluids **34**, 033103 (2022); https://doi.org/10.1063/5.0086511
Submitted: 26 January 2022 • Accepted: 19 February 2022 • Published Online: 09 March 2022

Evgenios Gryparis and Georgios C. Georgiou

Physics of Fluids ARTICLE scitation.org/journal/phf

Annular Poiseuille flow of Bingham fluids with wall slip

Cite as: Phys. Fluids **34**, 033103 (2022); doi: 10.1063/5.0086511
Submitted: 26 January 2022 · Accepted: 19 February 2022 ·
Published Online: 9 March 2022

Evgenios Gryparis[a] and Georgios C. Georgiou[b]

AFFILIATIONS

Department of Mathematics and Statistics, University of Cyprus, P.O. Box 20537, 1678 Nicosia, Cyprus

[a]E-mail: gryparis.evgenios@ucy.ac.cy
[b]Author to whom correspondence should be addressed: georgios@ucy.ac.cy

ABSTRACT

We consider the annular Poiseuille flow of a Bingham fluid with wall slip. First, the analytical solution is derived for the case in which Navier-slip conditions are applied at the two cylinders. A sliding (pure plug) regime is observed below a critical pressure gradient, and a yielding regime is eventually encountered above another critical pressure gradient in which the material yields near the two walls and moves as a plug in a core region. An intermediate semi-sliding regime is observed when different slip laws apply at the two walls in which the material yields only near the wall corresponding to weaker slip and the unyielded plug slides along the other. Next, we consider the case where wall slip occurs above a critical wall shear stress, the slip yield stress, which is taken to be less than the yield stress, in agreement with experimental observations. In this case, a no-flow regime is observed below a critical pressure gradient, followed by the sliding and yielding regimes. The critical values of the pressure gradient defining the various flow regimes are determined, and the closed-form solutions are provided for all cases. These are compared with available theoretical and experimental results in the literature.

I. INTRODUCTION

Yield-stress or viscoplastic materials are encountered in many processes of industrial interest, such as in pharmaceutics, cosmetics, food processing, oil drilling and transport, construction, and waste management, as well as in biophysical and geophysical processes.[1–4] These include various types of materials, such as concentrated suspensions, colloidal gels, emulsions, foams, pastes, drilling fluids, granular materials, nanocomposites, slurries, semisolid materials, biofluids (e.g., blood), and geomaterials.[5,6] Comprehensive reviews of viscoplasticity have been reported by Barnes,[1] Balmforth *et al.*,[2] Coussot,[3,5] Malkin *et al.*,[4] and Frigaard.[7]

Ideal viscoplastic materials behave as elastic solids when the applied stress is below a threshold value, the yield stress, τ_y^*; once the latter value is exceeded, the material behaves as a liquid. This dual behavior can be described by a two-branch constitutive law, such as the Bingham-plastic model,[8] the scalar form of which reads as follows:

$$\begin{cases} \dot{\gamma}^* = 0, & \tau^* \le \tau_y^*, \\ \tau^* = \tau_y^* + \mu^* \dot{\gamma}^*, & \tau^* > \tau_y^*, \end{cases} \tag{1}$$

where τ^* is the shear stress, $\dot{\gamma}^*$ is the shear rate, and μ^* is the plastic viscosity. It should be noted that throughout this paper stars denote dimensional quantities. The two-branch form of the viscoplastic constitutive equation requires the determination of the so-called yielded (fluid) and unyielded (rigid) regions of the flow field, corresponding, respectively, to $\tau^* > \tau_y^*$ and $\tau^* \le \tau_y^*$. The Newtonian model is recovered by setting $\tau_y^* = 0$. A popular generalization of the Bingham model is the Herschel–Bulkley model, which is a combination of the Bingham and power-law models.[9] Being non-linear, this model rules out the possibility of deriving analytical solutions in many rheometric flows of interest, with the exception of certain values of the power-law exponent.

It is well established that yield stress materials tend to slip at the walls.[1,10] As noted by Wilms *et al.*,[11] the apparent wall slip is an integral part of the pressure-driven flow of concentrated suspensions. In the case of suspensions, this phenomenon is attributed to the formation of a depleted slip layer near the wall where the particle concentration is much lower than in the bulk, which results in a steep velocity gradient interpreted as apparent slip.[1,12,13] The slip velocity, u_w^*, defined as the relative velocity of the fluid particles adjacent to a wall with respect to that of the wall, is assumed to be a function of the wall shear stress, τ_w^*. The simplest slip equation is the one proposed by Navier,[14]

$$\tau_w^* = \beta^* u_w^*, \tag{2}$$

where β^* is the slip coefficient, which generally varies with temperature, normal stress and pressure, the fluid properties, the materials of construction, and the wall surface characteristics.[15,16] Ortega-Avila *et al.*[12] note, in particular, that the slip coefficient depends on the slip layer thickness and the viscosity of the fluid constituting this layer. It should be noted that wall slip becomes stronger as β^* is reduced. When $\beta^* \to \infty$, Eq. (2) becomes equivalent to the no-slip boundary condition ($u_w^* = 0$), while when $\beta^* = 0$ "full slip" is achieved. Navier's slip law is generalized to the power-law model[15]

$$\tau_w^* = \beta^* u_w^{*s}, \tag{3}$$

where s is the exponent, also referred to as the slip index.[17] This model is often employed with viscoplastic microgels[16] and highly concentrated suspensions.[11]

Experiments indicate that slip is usually observed above a threshold value of the wall shear stress, τ_c^*, which is called sliding or slip yield stress.[15,18] Thus, Eq. (3) is further generalized as follows:

$$\begin{cases} u_w^* = 0, & \tau_w^* \le \tau_c^*, \\ \tau_w^* = \tau_c^* + \beta^* u_w^{*s}, & \tau_w^* > \tau_c^*. \end{cases} \tag{4}$$

Equation (4) has been employed for various yield-stress materials, for example, for Carbopol gels[19] and hard-sphere colloidal suspensions.[20] Notwithstanding the obvious exception of non-viscoplastic generalized Newtonian fluids, for example, Newtonian and power-law fluids, exhibiting slip with non-zero slip yield stress, to our knowledge, in all experimental reports on viscoplastic materials, the slip yield stress is below the yield stress (see Ref. 21 and references therein).

The dual behavior of slip equation (4) is similar to that of the Bingham plastic constitutive equation. Different flow regimes are observed depending on the relative values of the yield stress τ_y^* and the slip yield stress τ_c^*. The number of these different regimes increases in rheometric flows with two characteristic wall shear stresses, such as the circular Couette and the annular Poiseuille flows. As a result of slip, the apparent shear rate does not coincide with the apparent shear rate and their difference is geometry dependent; for example, it varies with the gap size in a Couette rheometer. Therefore, slip effects need to be accounted for in order to obtain reliable estimates of the rheological parameters.[15,22] This is more crucial with yield stress fluids due to the heterogeneous nature of their flow profile, since regions of slip-, shear-, and plug flow can co-exist instead of pure shear flow.[17] Yield stress fluids may also slide in the presence of slip[21,23] in which case the actual shear rate is zero, while the apparent one is finite.

Recently, analytical solutions of certain viscometric flows of viscoplastic materials exhibiting wall slip with non-zero slip yield stress have been reported in the literature. These include the parallel plate flow Herschel–Bulkley fluids,[20,24] the axisymmetric Poiseuille flow of a Herschel–Bulkley fluid,[25] and the Couette flow of a Bingham plastic.[21] In all the above works, different flow regimes were identified along with the critical conditions defining the transition from one regime to the other.

The objective of the present paper is to analyze the implications of wall slip on the apparent flow curve in the case of steady annular Poiseuille flow of a Bingham plastic. This flow is of interest in oil-drilling, food processing, wire coating, etc.[26] We investigate, in particular, the effects of applying different slip laws at the inner and outer cylinders and of non-zero slip yield stress.

The analytical solution of fully developed flow of a Bingham fluid in a concentric annular tube has been derived in the classical papers of Fredrickson and Bird[27] under the assumption of no slip; see also Ref. 28. Brunn and Abu-Jdayil[29] solved the same flow for a Bingham fluid with position-dependent yield stress, akin to electro- and magnetorheological fluids. Ioannou and Georgiou[30] derived a semi-analytical solution of the annular Poiseuille flow of a Bingham fluid with pressure-dependent plastic viscosity and yield stress for the special case where both parameters vary linearly with pressure with the same growth coefficient. More recently, Huilgol and Georgiou[31] proposed a fast numerical scheme for solving the annular Poiseuille flow of non-Newtonian fluids, including Bingham and Herschel–Bulkley fluids.

Ortega-Avila *et al.*[12] studied both experimentally and numerically the annular flow of a Herschel–Bulkley fluid in the presence of wall slip for which there is no analytical solution, with the exception of certain values of the power-law exponent. However, they considered only the case where the same slip law with zero slip yield stress applies along the two cylinders. They thus identified two flow regimes, the sliding (plug-flow) and yielding regimes depending on whether the absolute values of the shear stresses at the two walls were below or above the yield stress. Ortega-Avila *et al.*[12] obtained velocity distributions within the annulus by means of particle image velocimetry and compared them with their numerical predictions for fully developed flow. They also reported that, for high values of the radii ratio (i.e., for small gaps), the slip velocities as well as the absolute values of the wall shear stress were similar, and thus, the flow is viscometric. Chatzimina *et al.*[32] investigated the annular Poiseuille flow a Newtonian fluid in the presence of slip. They employed different slip models and investigated the flow stability; in the case, a non-monotonic slip is equation is applied at the two walls. Also, Ferrás *et al.*[26] provided analytical and numerical solutions for axial and helical flows of linear, quadratic, and exponential Phan-Thien–Tanner viscoelastic fluids under no-slip and slip boundary conditions.

In Sec. II, the annular Poiseuille flow of a Bingham plastic is analyzed and general expressions for the solution are presented in terms of the two slip velocities, which are independent from the slip laws applied at the two walls. More specifically, the solutions below a critical pressure gradient where the material moves as a solid (sliding or pure-plug regime) and above another critical value, where the material yields near both walls and moves as a plug in an intermediate annular core (yielding regime) are provided. In Sec. III, we analyze the flow in the case when different Navier laws apply on the two cylinders. Considering different slip equations may be justified even when the materials of construction of the two walls are the same. The thickness of the apparent slip layer changes with the wall shear stress,[12,33] and thus, the corresponding slip coefficients may be different, especially if the annular gap is not small. It is demonstrated that there exists an intermediate semi-sliding regime between the sliding and yielding regimes in which the material yields only near the wall of weaker slip and slides unyielded along the other. Then, in Sec. IV, we consider the case of non-zero slip yield stress, but for the sake of simplicity, it is assumed that the same slip law applies at the two walls. In this case, the no-flow regime is followed by the sliding and yielding regimes. The critical pressure gradients defining the various regimes are obtained and comparisons are made with available results in the literature.

II. GENERAL SOLUTION

Consider the steady flow between infinitely long, coaxial cylinders of inner and outer radii κR^* and R^*, where $0 < \kappa < 1$, driven by a pressure gradient G^* in the positive z-direction. Integrating the z-momentum equation for any generalized Newtonian fluid gives

$$\tau^*_{rz} = -\frac{G^* r^*}{2} + \frac{c^*}{r^*}, \tag{5}$$

where c^* is an integration constant determined from any of the two boundary conditions for the axial velocity. Upon observing that the shear stress is positive in the interval $[\kappa R^*, \lambda R^*)$ and negative in $(\lambda R^*, R^*]$, where $\kappa < \lambda < 1$,[31] the constant c^* can be replaced by λ, such that the shear stress τ^*_{rz} vanishes at $r^* = \lambda R^*$. Thus, one finds that[27]

$$\tau^*_{rz} = \frac{G^* R^*}{2}\left(\frac{\lambda^2 R^*}{r^*} - \frac{r^*}{R^*}\right). \tag{6}$$

Hence, the wall shear stresses at the inner and outer cylinders, respectively, read

$$\tau^*_{w1} = |\tau^*_{rz}(\kappa R^*)| = \tau^*_{rz}(\kappa R^*) = \frac{G^* R^*}{2\kappa}(\lambda^2 - \kappa^2) \tag{7}$$

and

$$\tau^*_{w2} = |\tau^*_{rz}(R^*)| = -\tau^*_{rz}(R^*) = \frac{G^* R^*}{2}(1 - \lambda^2). \tag{8}$$

The above equations hold for any generalized Newtonian fluid and are independent of the boundary conditions. In this section, we derive generic expressions of the solution in terms of the two slip velocities $u^*_{w1} = u^*(\kappa R^*)$ and $u^*_{w2} = u^*(R^*)$.

Assume now that the fluid is viscoplastic with yield stress τ^*_y. In the general case, a sliding, a semi-sliding, and a yielding regime may be observed, which are defined by two critical values, G^*_1 and G^*_2, of the pressure gradient. In the sliding (or pure-plug) regime ($G^* \le G^*_1$), there is no deformation in the bulk; the material slides unyielded (i.e., as a solid) at a constant velocity, and thus, the two slip velocities are equal. In the no-slip case, the material remains stationary. Bulk deformation only starts when $G^* > G^*_2$ (yielding regime); the material is yielded near the walls and unyielded in an intermediate annular core where the velocity is flat. When the same slip law is applied at both cylinders, $G^*_1 = G^*_2$. Thus, an intermediate semi-sliding regime ($G^*_1 < G^* \le G^*_2$) is observed only when different slip laws apply at the two walls. This also includes the cases where slip occurs only along one cylinder. In the semi-sliding regime, the material yields only near the wall of weaker slip and slides unyielded along the other; that is, the plug extends until the wall where slip is stronger. The sliding and yielding regimes are discussed below. The semi-sliding regime is analyzed in Sec. III, where different Navier slip laws are considered at the two walls.

In the sliding regime ($G^* \le G^*_1$), the slip velocities at the two cylinders are equal and the velocity and the volumetric flow rate are given by

$$u^*(r^*) = u^*_{w1} = u^*_{w2}, \quad G^* \le G^*_1 \tag{9}$$

and

$$Q^* = \pi u^*_{w1} R^{*2}(1 - \kappa^2), \quad G^* \le G^*_1. \tag{10}$$

In the yielding regime ($G^* > G^*_2$), the material yields near both the walls and remains unyielded in an intermediate region, as illustrated in Fig. 1. In Regions I and II corresponding, respectively, to $\kappa R^* < r^* < \lambda_1 R^*$ and $\lambda_2 R^* < r^* < R^*$, where $\kappa < \lambda_1 < \lambda_2 < 1$, the material is yielded. In the intermediate Region III ($\lambda_1 R^* \le r^* \le \lambda_2 R^*$), the material is unyielded and moves as a solid with a constant velocity. Substituting $\tau^*_{rz}(\lambda_1 R^*) = -\tau^*_{rz}(\lambda_2 R^*) = \tau^*_y$ into Eq. (6), one finds that

$$\lambda_1 \lambda_2 = \lambda^2 \quad \text{and} \quad \lambda_2 - \lambda_1 = 2Bn, \tag{11}$$

where

$$Bn \equiv \frac{\tau^*_y}{G^* R^*} \tag{12}$$

is the Bingham number, which can also be viewed as an inverse dimensionless pressure gradient, $G = 1/Bn \equiv G^* R^*/\tau^*_y$. By means of Eq. (11), the two wall shear stresses in Eqs. (7) and (8) can be written as follows:

$$\tau^*_{w1} = \frac{G^* R^*}{2\kappa}\left[\lambda_2(\lambda_2 - 2Bn) - \kappa^2\right] = \frac{\tau^*_y}{2\kappa Bn}\left[\lambda_2(\lambda_2 - 2Bn) - \kappa^2\right] \tag{13}$$

and

$$\tau^*_{w2} = \frac{G^* R^*}{2}\left[1 - \lambda_2(\lambda_2 - 2Bn)\right] = \frac{\tau^*_y}{2Bn}\left[1 - \lambda_2(\lambda_2 - 2Bn)\right]. \tag{14}$$

The analysis, which up to this point holds for any yield-stress fluid, continues below for the special case of a Bingham fluid. The analysis for a Herschel–Bulkley fluid can be found in Refs. 12 and 31. There is no analytical solution for the velocity in the general case, except for certain values of the power-law exponent, for example, when $1/n$ is integer.

In Region I, the velocity derivative is positive, and thus, $\tau^*_{rz} = \tau^*_y + \mu^* du^*/dr^*$. Substituting into Eq. (6) gives

$$\frac{du^*_I}{dr^*} = \frac{G^* R^*}{2\mu^*}\left(\frac{\lambda^2 R^*}{r^*} - \frac{r^*}{R^*} - 2Bn\right), \tag{15}$$

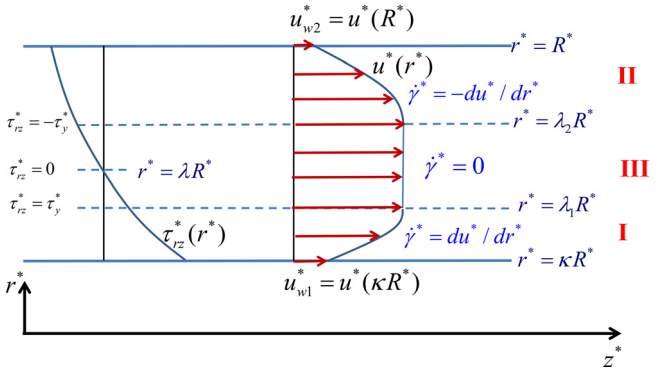

FIG. 1. Geometry and boundary conditions of annular viscoplastic Poiseuille flow with wall slip. Above a critical pressure, there are two yielded regions (I and II) adjacent to the walls and an unyielded annular core (region III).

which upon integration and application of the condition $u_I^*(\kappa R^*) = u_{w1}^*$ gives

$$u_I^*(r^*) = u_{w1}^* + \frac{G^* R^{*2}}{4\mu^*}\left[2\lambda^2 \ln\frac{r^*}{\kappa R^*} - \frac{r^{*2}}{R^{*2}} + \kappa^2 - 4Bn\left(\frac{r^*}{R^*} - \kappa\right)\right], \quad \kappa R^* \le r^* \le \lambda_1 R^*. \tag{16}$$

In Region II, the velocity derivative is negative, and thus, $\tau_{rz}^* = -\tau_y^* + \mu^* du^*/dr^*$ and

$$\frac{du_{II}^*}{dr^*} = -\frac{G^* R^*}{2\mu^*}\left(-\frac{\lambda^2 R^*}{r^*} + \frac{r^*}{R^*} - 2Bn\right). \tag{17}$$

Integrating and applying $u_{II}^*(R^*) = u_{w2}^*$ give

$$u_{II}^*(r^*) = u_{w2}^* + \frac{G^* R^{*2}}{4\mu^*}\left[-2\lambda^2 \ln\frac{R^*}{r^*} + 1 - \frac{r^{*2}}{R^{*2}} - 4Bn\left(1 - \frac{r^*}{R^*}\right)\right], \quad \lambda_2 R^* \le r^* \le R^*. \tag{18}$$

The velocity of the unyielded core (Region III) is $u_{III}^*(r^*) = u_I^*(\lambda_1 R^*) = u_{II}^*(\lambda_2 R^*)$, which leads to the following condition:

$$u_{w1}^* - u_{w2}^* = \frac{G^* R^{*2}}{4\mu^*}\left[-2\lambda^2 \ln\frac{\lambda_1}{\kappa} + \lambda_1^2 - \kappa^2 + 4Bn(\lambda_1 - \kappa) - 2\lambda^2 \ln\frac{1}{\lambda_2} + 1 - \lambda_2^2 - 4Bn(1 - \lambda_2)\right]. \tag{19}$$

Equation (19) is further simplified by means of Eq. (11) to the following non-linear equation for λ_2:

$$2\lambda_2(\lambda_2 - 2Bn)\ln\frac{\lambda_2 - 2Bn}{\kappa\lambda_2} - 1 + 4Bn(1 - \lambda_2) + (2Bn + \kappa)^2 + \frac{4\mu^*}{G^* R^{*2}}(u_{w1}^* - u_{w2}^*) = 0. \tag{20}$$

The velocity profile when $G^* > G_2^*$ can be written as follows:

$$u^*(r^*) = \begin{cases} u_{w1}^* + \dfrac{G^* R^{*2}}{4\mu^*}\left[2\lambda^2 \ln\dfrac{r^*}{\kappa R^*} - \dfrac{r^{*2}}{R^{*2}} + \kappa^2 - 4Bn\left(\dfrac{r^*}{R^*} - \kappa\right)\right], & \kappa R^* \le r^* \le \lambda_1 R^*, \\ u_{w1}^* + \dfrac{G^* R^{*2}}{4\mu^*}\left[2\lambda^2 \ln\dfrac{\lambda_1}{\kappa} - \lambda_1^2 + \kappa^2 - 4Bn(\lambda_1 - \kappa)\right], & \lambda_1 R^* \le r^* \le \lambda_2 R^*, \quad G^* > G_2^*, \\ u_{w2}^* + \dfrac{G^* R^{*2}}{4\mu^*}\left[-2\lambda^2 \ln\dfrac{R^*}{r^*} + 1 - \dfrac{r^{*2}}{R^{*2}} - 4Bn\left(1 - \dfrac{r^*}{R^*}\right)\right], & \lambda_2 R^* \le r^* \le R^*. \end{cases} \tag{21}$$

For the volumetric flow rate, it is easily demonstrated that

$$Q^* = 2\pi\int_{\kappa R^*}^{R^*} u^*(r^*) r^* dr^* = \pi R^{*2}\left(u_{w2}^* - \kappa^2 u_{w1}^*\right) - \pi\int_{\kappa R^*}^{R^*} \frac{du^*}{dr^*} r^{*2} dr^*. \tag{22}$$

Since the unyielded region has zero contribution to the last integral,

$$Q^* = \pi R^{*2}\left(u_{w2}^* - \kappa^2 u_{w1}^*\right) - \pi\int_{\kappa R^*}^{\lambda_1 R^*} \frac{du_I^*}{dr^*} r^{*2} dr^* - \pi\int_{\lambda_2 R^*}^{R^*} \frac{du_{II}^*}{dr^*} r^{*2} dr^*, \tag{23}$$

which gives

$$Q^* = \pi R^{*2}\left(u_{w2}^* - \kappa^2 u_{w1}^*\right) + \frac{\pi G^* R^{*4}}{2\mu^*}\left[\frac{1}{4}\left(\lambda_1^4 - \kappa^4\right) + \frac{2Bn}{3}\left(\lambda_1^3 - \kappa^3\right) - \frac{\lambda^2}{2}\left(\lambda_1^2 - \kappa^2\right) + \frac{1}{4}\left(1 - \lambda_2^4\right) - \frac{2Bn}{3}\left(1 - \lambda_2^3\right) - \frac{\lambda^2}{2}\left(1 - \lambda_2^2\right)\right], \tag{24}$$

and by means of Eq. (11),

$$Q^* = \pi R^{*2}\left(u_{w2}^* - \kappa^2 u_{w1}^*\right) + \frac{\pi G^* R^{*4}}{8\mu^*}\left[1 - \kappa^4 - 2(1 - \kappa^2)(\lambda_2 - 2Bn)\lambda_2 - \frac{8}{3}(1 + \kappa^3)Bn + \frac{16}{3}(\lambda_2 - Bn)^3 Bn\right], \quad G^* > G_2^*. \tag{25}$$

The slip velocities that appear in the above equations are calculated by means of the governing slip law. Setting the two slip velocities to zero yields the special cases of Eqs. (20) and (25) for the no-slip case.[28,34]

A. Non-dimensionalization

For convenience, we will nondimensionalize the flow variables as follows:

$$r \equiv \frac{r^*}{R^*}, \quad u \equiv \frac{u^*}{\tau_y^* R^*/\mu^*}, \quad Q \equiv \frac{Q^*}{\pi\tau_y^* R^{*3}/\mu^*}, \quad \tau \equiv \frac{\tau^*}{\tau_y^*}, \quad G \equiv \frac{G^*}{\tau_y^*/R^*}. \tag{26}$$

It should be noted that with these scales the non-dimensional pressure gradient is now the inverse of the Bingham number; see Eq. (12). The dimensionless shear stress is given by [cf. Eq. (6)]

$$\tau_{rz} = \left(\frac{\lambda^2}{r} - r\right)\frac{G}{2}, \tag{27}$$

while the inner and outer wall shear stresses read

$$\tau_{w1} = (\lambda^2 - \kappa^2)\frac{G}{2\kappa} \quad \text{and} \quad \tau_{w2} = (1-\lambda^2)\frac{G}{2}. \tag{28}$$

In the sliding regime ($G \le G_1$), $u(r) = u_{w1} = u_{w2}$ and $Q = u_{w1}(1-\kappa^2)$. In the yielding regime ($G > G_2$), λ_1 and λ_2 satisfy

$$\lambda_1\lambda_2 = \lambda^2 \quad \text{and} \quad \lambda_2 - \lambda_1 = \frac{2}{G}, \tag{29}$$

and the wall shear stresses are given by

$$\begin{aligned} \tau_{w1} &= \frac{G}{2\kappa}\left[\lambda_2\left(\lambda_2 - \frac{2}{G}\right) - \kappa^2\right] \quad \text{and} \\ \tau_{w2} &= \frac{G}{2}\left[1 - \lambda_2\left(\lambda_2 - \frac{2}{G}\right)\right], \quad G > G_2. \end{aligned} \tag{30}$$

Hence, the nonlinear equation to be solved for λ_2 [taking Eq. (29) into account] becomes

$$\begin{aligned} &2\lambda^2 \ln\frac{\lambda_1}{\kappa\lambda_2} - \lambda_1^2 + \kappa^2 - \frac{4}{G}(\lambda_1 - \kappa) - 1 + \lambda_2^2 \\ &+ \frac{4}{G}(1-\lambda_2) + \frac{4}{G}(u_{w1} - u_{w2}) = 0, \end{aligned} \tag{31}$$

or

$$2\lambda^2 \ln\frac{\lambda_1}{\kappa\lambda_2} - 1 + \frac{4}{G}(1-\lambda_2) + \left(\frac{2}{G} + \kappa\right)^2 + \frac{4}{G}(u_{w1} - u_{w2}) = 0. \tag{32}$$

The velocity and the volumetric flow rate are given by

$$u(r) = \begin{cases} u_{w1} + \dfrac{G}{4}\left[2\lambda^2 \ln\dfrac{r}{\kappa} - r^2 + \kappa^2 - \dfrac{4}{G}(r-\kappa)\right], & \kappa \le r \le \lambda_1, \\ u_{w1} + \dfrac{G}{4}\left[2\lambda^2 \ln\dfrac{\lambda_1}{\kappa} - \lambda_1^2 + \kappa^2 - \dfrac{4}{G}(\lambda_1 - \kappa)\right], & \lambda_1 \le r \le \lambda_2, \\ u_{w2} + \dfrac{G}{4}\left[-2\lambda^2 \ln\dfrac{1}{r} + 1 - r^2 - \dfrac{4}{G}(1-r)\right], & \lambda_2 \le r \le 1, \end{cases} \tag{33}$$

and

$$\begin{aligned} Q = \frac{G}{2}\Bigg[&\frac{1}{4}\left(\lambda_1^4 - \kappa^4\right) + \frac{2}{3G}\left(\lambda_1^3 - \kappa^3\right) - \frac{\lambda^2}{2}\left(\lambda_1^2 - \kappa^2\right) \\ &+ \frac{1}{4}\left(1 - \lambda_2^4\right) - \frac{2}{3G}\left(1 - \lambda_2^3\right) - \frac{\lambda^2}{2}\left(1 - \lambda_2^2\right)\Bigg] + u_{w2} - \kappa^2 u_{w1}, \end{aligned} \tag{34}$$

or

$$\begin{aligned} Q = \frac{G}{8}\Bigg[&1 - \kappa^4 - 2(1-\kappa^2)\lambda^2 - \frac{8}{3G}(1+\kappa^3) \\ &+ \frac{16}{3G}\left(\lambda_2 - \frac{1}{G}\right)^3\Bigg] + u_{w2} - \kappa^2 u_{w1}. \end{aligned} \tag{35}$$

III. NAVIER SLIP

In this section, we consider the case where Navier slip occurs at both walls, with slip coefficients β_1^* and β_2^*,

$$\tau_{wi} = \frac{1}{B_i}u_{wi}, \quad i = 1, 2, \tag{36}$$

where

$$B_i = \frac{\mu^*}{\beta_i^* R^*}, \quad i = 1, 2, \tag{37}$$

are the dimensionless slip numbers. Note that $B_i = 0$ implies no-slip at the corresponding wall. Substituting Eq. (36) into Eq. (28), we find the following expressions for the two slip velocities:

$$u_{w1} = \frac{B_1 G}{2\kappa}(\lambda^2 - \kappa^2), \quad u_{w2} = \frac{B_2 G}{2}(1-\lambda^2), \tag{38}$$

and, thus,

$$u_{w1} - u_{w2} = \left[\frac{B_1}{\kappa}(\lambda^2 - \kappa^2) - B_2(1-\lambda^2)\right]\frac{G}{2} \tag{39}$$

and

$$u_{w2} - \kappa^2 u_{w1} = \left[B_2(1-\lambda^2) - B_1\kappa(\lambda^2 - \kappa^2)\right]\frac{G}{2}. \tag{40}$$

A. Sliding regime

In the sliding regime ($G \le G_1$), the slip velocities are equal and Eq. (38) yields

$$\lambda^2 = \frac{\kappa(\kappa B_1 + B_2)}{B_1 + \kappa B_2}. \tag{41}$$

Substituting λ^2 back to Eq. (38), one gets

$$u = u_{w1} = u_{w2} = \frac{B_1 B_2 (1-\kappa^2) G}{2(B_1 + \kappa B_2)}, \quad G \le G_1. \tag{42}$$

Also, the two wall shear stresses are

$$\tau_{w1} = \frac{B_2(1-\kappa^2)G}{2(B_1 + \kappa B_2)} \quad \text{and} \quad \tau_{w2} = \frac{B_1(1-\kappa^2)G}{2(B_1 + \kappa B_2)}, \quad G \le G_1. \tag{43}$$

The volumetric flow rate is then given by

$$Q = \frac{B_1 B_2 (1-\kappa^2)^2 G}{2(B_1 + \kappa B_2)}, \quad G \le G_1. \tag{44}$$

When the same slip law applies at the two walls ($B_1 = B_2$), the wall shear stresses τ_{w1} and τ_{w2} remain equal as the imposed pressure gradient G is increased. Hence, the fluid yields at both walls when $G = G_1$. If, however, the slip laws differ, the material first yields at the wall where slip is weaker and the corresponding wall shear stress is bigger. Hence, the material yields first at the inner or outer cylinder depending on whether $B_1 < B_2$ or $B_1 > B_2$, and G_1 is smaller than the critical pressure gradient G_2 at which yielding occurs near both walls. The three cases may be summarized as follows:

(a) When $B_1 = B_2$, $G_1 = G_2$ and the sliding regime $(0, G_1]$ is followed by the yielding regime (G_1, ∞), as illustrated in Fig. 2(a).
(b) When $B_1 < B_2$, the sliding regime $(0, G_1]$ is followed by a semi-sliding regime $(G_1, G_2]$ where the material yields only near the inner cylinder and slides along the outer one, as shown in Fig. 2(b). In other words, Region II is not observed and appears only above G_2.
(c) When $B_1 > B_2$, we have the three regimes shown in Fig. 2(c). In the semi-sliding regime $(G_1, G_2]$, Region I is not observed and the material yields near the outer wall and slides along the inner wall.

Before analyzing the above three cases and obtaining the corresponding critical values of the pressure gradient, we discuss the yielding regime, which is present in all cases.

B. Yielding regime

The velocity profile in the yielding regime $(G > G_2)$ is given by Eq. (33). Upon substitution of the slip velocities from Eq. (39), Eq. (32) for λ_2 becomes

$$2\lambda^2 \ln\frac{\lambda_1}{\kappa\lambda_2} - 1 + \frac{4}{G}(1-\lambda_2) + \left(\frac{2}{G}+\kappa\right)^2 + 2\left[\frac{B_1}{\kappa}(\lambda^2-\kappa^2) - B_2(1-\lambda^2)\right] = 0, \quad G > G_2. \tag{45}$$

Similarly, substituting Eq. (40) into Eq. (35), the following expression is obtained for the volumetric flow rate:

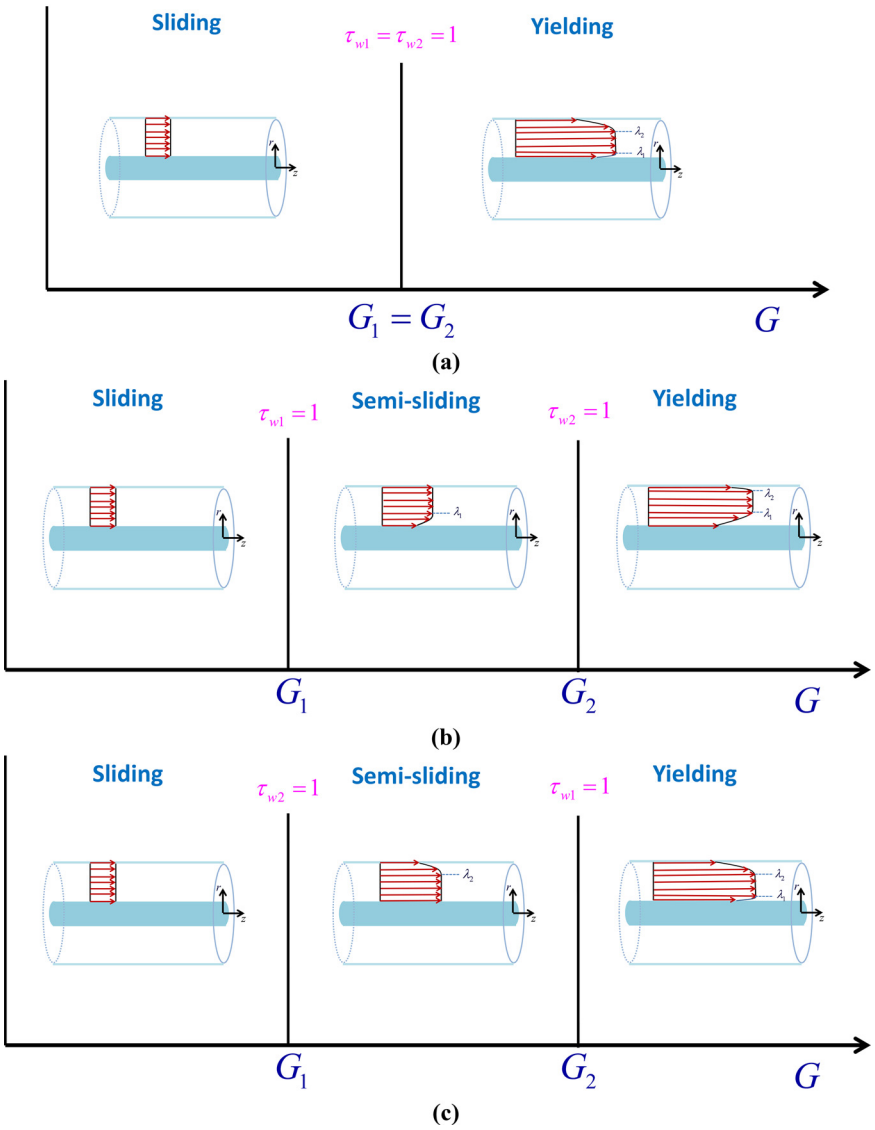

FIG. 2. Flow regimes of annular viscoplastic Poiseuille flow with Navier wall slip (zero slip yield stress) when: (a) the same slip law applies at the two cylinders; (b) slip at the inner cylinder is weaker; (c) slip at the inner cylinder is stronger.

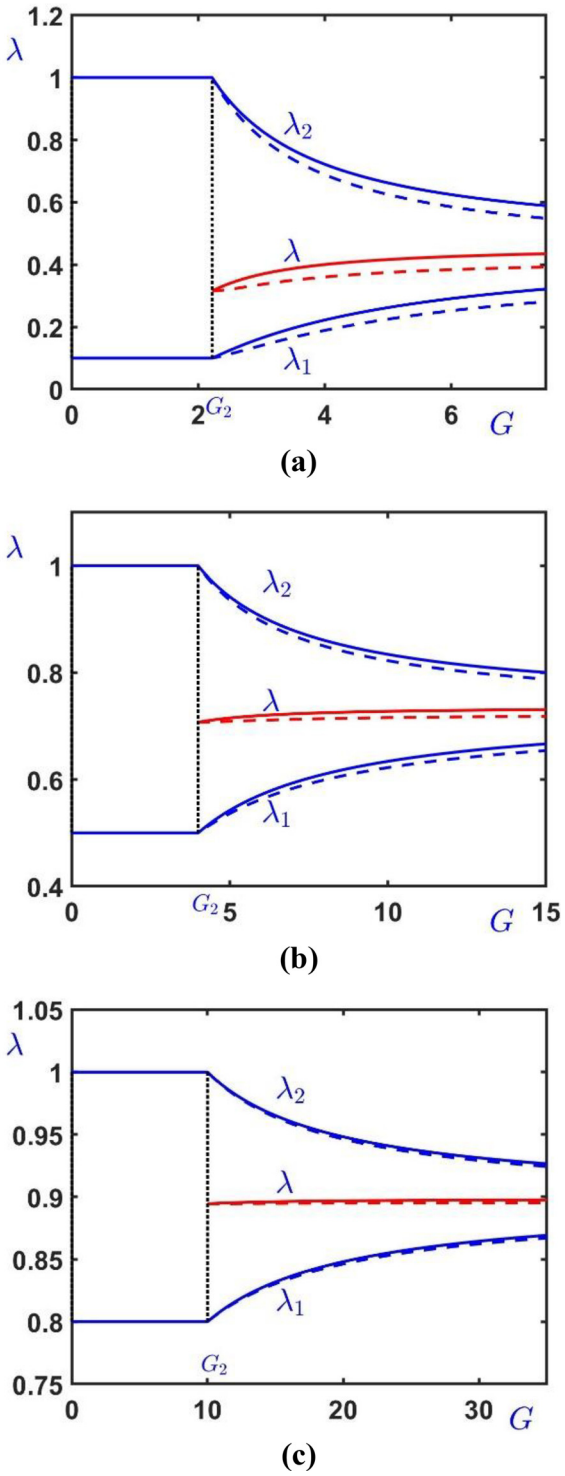

FIG. 3. Effect of Navier slip on the dimensionless yield radii λ_1 and λ_2 and the radius λ of zero shear stress. The solid lines correspond to $B = 0$ (no slip, solid lines) and $B = 0.1$ (strong slip, dashed lines): (a) $\kappa = 0.1$; (b) $\kappa = 0.5$; (c) $\kappa = 0.8$. λ increases from the value of $\sqrt{\kappa}$ at $G = G_1$ to the limiting value λ_N of Eq. (56) as $G \to \infty$.

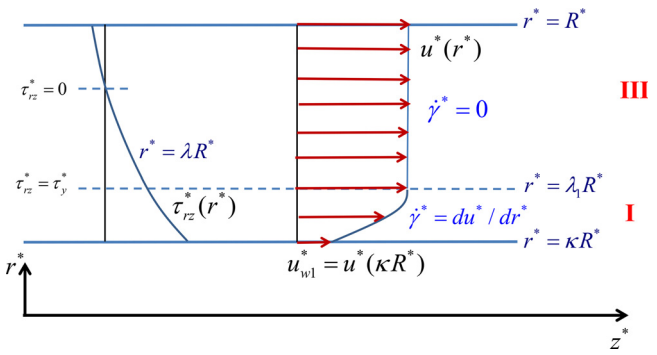

FIG. 4. Velocity profile in the semi-sliding regime when wall slip is weaker at the inner cylinder. The material yields only near the inner cylinder and slides along the external one; Region II is not observed.

$$Q = \frac{G}{8}\left[1 - \kappa^4 - 2(1-\kappa^2)\lambda^2 - \frac{8}{3G}(1+\kappa^3) + \frac{16}{3G}\left(\lambda_2 - \frac{1}{G}\right)^3 + 4B_2(1-\lambda^2) - 4B_1\kappa(\lambda^2 - \kappa^2)\right]. \quad (46)$$

At high pressure gradients, the solution tends asymptotically to the Newtonian one. Setting $G \to \infty$ and $\lambda_1 = \lambda_2 = \lambda$ (so that Region III disappears) in Eq. (45), we find that

$$\lambda_N = \sqrt{\frac{1 - \kappa^2 + 2(\kappa B_1 + B_2)}{2[\ln(1/\kappa) + B_1/\kappa + B_2]}}. \quad (47)$$

Substituting the above value into Eq. (46), we find the Newtonian volumetric flow rate

$$Q_N = \frac{G}{8}\left\{1 - \kappa^4 + 4(B_1\kappa^3 + B_2) - \frac{\left[1 - \kappa^2 + 2(\kappa B_1 + B_2)\right]^2}{\ln(1/\kappa) + B_1/\kappa + B_2}\right\}. \quad (48)$$

At high values of the pressure gradient, the volumetric flow rate in Eq. (46) may also be approximated by setting $\lambda_1 = \lambda_2 = \lambda_N$ (the plug region is small compared with the dimensions of the annulus),

$$Q \approx \frac{G}{8}\left[1 - \kappa^4 - 2(1-\kappa^2)\lambda_N^2 - \frac{8}{3G}(1+\kappa^3) + \frac{16}{3G}\lambda_N^3 + 4B_2(1-\lambda_N^2) - 4B_1\kappa(\lambda_N^2 - \kappa^2)\right]. \quad (49)$$

This expression generalizes the approximation obtained by Fredrickson and Bird[27] for the no-slip case.

C. Same slip laws along the two walls ($B_1 = B_2$)

If the same slip law applies at the two cylinders, then in the sliding regime $\tau_{w1} = \tau_{w2}$. The critical pressure gradient above which the fluid yields (at both walls) corresponds to $\tau_{w1} = \tau_{w2} = 1$ and hence from Eq. (28) one obtains $\lambda^2 = \kappa$,

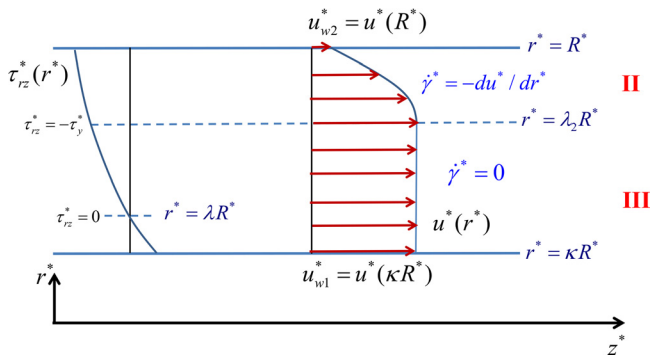

FIG. 5. Velocity profile in the semi-sliding regime when wall slip at the inner cylinder is stronger. The material yields only near the outer cylinder and slides along the internal one; Region I is not observed.

$$\tau_{w1} = \tau_{w2} = \frac{1}{2}(1-\kappa)G, \quad G_1 \le G \le G_2, \tag{50}$$

and

$$G_1 = G_2 = \frac{2}{1-\kappa}. \tag{51}$$

In fact, Eq. (51) holds for any yield-stress fluid. Given that $B_1 = B_2 = B$, where $B = \eta^*/(\beta^* R^*)$ is the slip number, the velocity and the volumetric flow rate in the sliding regime become

$$u = \frac{B}{2}(1-\kappa)G, \quad 0 \le G \le G_1, \tag{52}$$

and

$$Q = \frac{B}{2}(1+\kappa)(1-\kappa)^2 G, \quad 0 \le G \le G_1. \tag{53}$$

In the yielding regime, that is, for $G > G_1 = G_2$, Eqs. (45) and (46) are simplified as follows:

$$2\lambda^2 \ln\frac{\lambda_1}{\kappa\lambda_2} - 1 + \frac{4}{G}(1-\lambda_2) + \left(\frac{2}{G}+\kappa\right)^2 + 2B(1+1/\kappa)(\lambda^2-\kappa) = 0, \quad G > G_2 \tag{54}$$

and

$$Q = \frac{G}{8}\left\{1-\kappa^4 - 2(1-\kappa^2)\lambda^2 - \frac{8}{3G}(1+\kappa^3) + \frac{16}{3G}\left(\lambda_2 - \frac{1}{G}\right)^3 + 4B\left[1+\kappa^3-(1+\kappa)\lambda^2\right]\right\}, \quad G > G_2. \tag{55}$$

Equations (47) and (48) for the Newtonian solution become

$$\lambda_N = \sqrt{\frac{1-\kappa^2+2(1+\kappa)B}{2[\ln(1/\kappa)+(1+1/\kappa)B]}} \tag{56}$$

and

$$Q_N = \frac{G}{8}\left\{1-\kappa^4+4(1+\kappa^3)B - \frac{\left[1-\kappa^2+2(1+\kappa)B\right]^2}{\ln(1/\kappa)+(1+1/\kappa)B}\right\}. \tag{57}$$

The above expressions, though much simpler, are equivalent to the Newtonian solution reported in Ref. 32, where a less convenient definition of the slip number was used. It is easily shown that λ is an increasing function of the pressure gradient G, ranging from $\sqrt{\kappa}$ at $G = G_1$ to the limiting value λ_N of Eq. (56) as $G \to \infty$. This is illustrated in Fig. 3, where λ_1, λ_2, and λ are plotted vs the pressure gradient for $B = 0$ (no-slip) and $B = 0.1$(strong slip) and three different radii ratios ($\kappa = 0.1$, 0.5, and 0.8). One observes that as slip is increased, the unyielded region is shifted toward the inner cylinder.

D. Weaker slip at the inner wall ($B_1 < B_2$)

The semi-sliding regime is defined by the critical values G_1 and G_2 of the pressure gradient, which correspond to $\tau_{w1} = 1$ and $\tau_{w2} = 1$, respectively. G_1 is determined by means of Eq. (43),

$$G_1 = \frac{2(B_1+\kappa B_2)}{B_2(1-\kappa^2)}, \tag{58}$$

whereas G_2 will be determined below. Since the material adjacent to the outer cylinder is unyielded (no region II), λ_2 is not relevant (see Fig. 4). The velocity in $[G_1, G_2]$ is given by

$$u(r) = \begin{cases} u_{w1} + \dfrac{G}{4}\left[2\lambda^2\ln\dfrac{r}{\kappa} - r^2 + \kappa^2 - \dfrac{4}{G}(r-\kappa)\right], & \kappa \le r \le \lambda_1, \\ u_{w2}, & \lambda_1 \le r \le 1, \end{cases} \tag{59}$$

TABLE I. Critical pressure gradients when Navier slip applies at the two walls.

$B_1 = B_2$	$B_1 < B_2$	$B_1 > B_2$
No semi-sliding regime $G_1 = G_2 = \dfrac{2}{1-\kappa}$	Semi-sliding regime: $[G_1, G_2]$ $G_1 = \dfrac{2(B_1+\kappa B_2)}{B_2(1-\kappa^2)}$, $G_2 = \dfrac{2}{1-\lambda_c^2} = \dfrac{2}{1-\lambda_{1c}}\lambda_{1c}$ λ_{1c} is a root of Eq. (67)	Semi-sliding regime: $[G_1, G_2]$ $G_1 = \dfrac{2(B_1+\kappa B_2)}{B_1(1-\kappa^2)}$, $G_2 = \dfrac{2\kappa}{\lambda_c^2-\kappa^2} = \dfrac{2}{\lambda_{2c}-\kappa}\lambda_{2c}$ λ_{2c} is a root of Eq. (79)
If $B_1 = B_2 = 0$, no sliding in $[0, G_1]$	If $B_1 = 0$, no sliding in $[0, G_1]$ with $G_1 = \dfrac{2\kappa}{1-\kappa^2}$	If $B_2 = 0$, no sliding in $[0, G_1]$ with $G_1 = \dfrac{2}{1-\kappa^2}$
	If B_1 is finite and $B_2 \to \infty$ (full slip), $G_1 \to \dfrac{2\kappa}{1-\kappa^2}$	If B_2 is finite and $B_1 \to \infty$ (full slip), $G_1 \to \dfrac{2}{1-\kappa^2}$

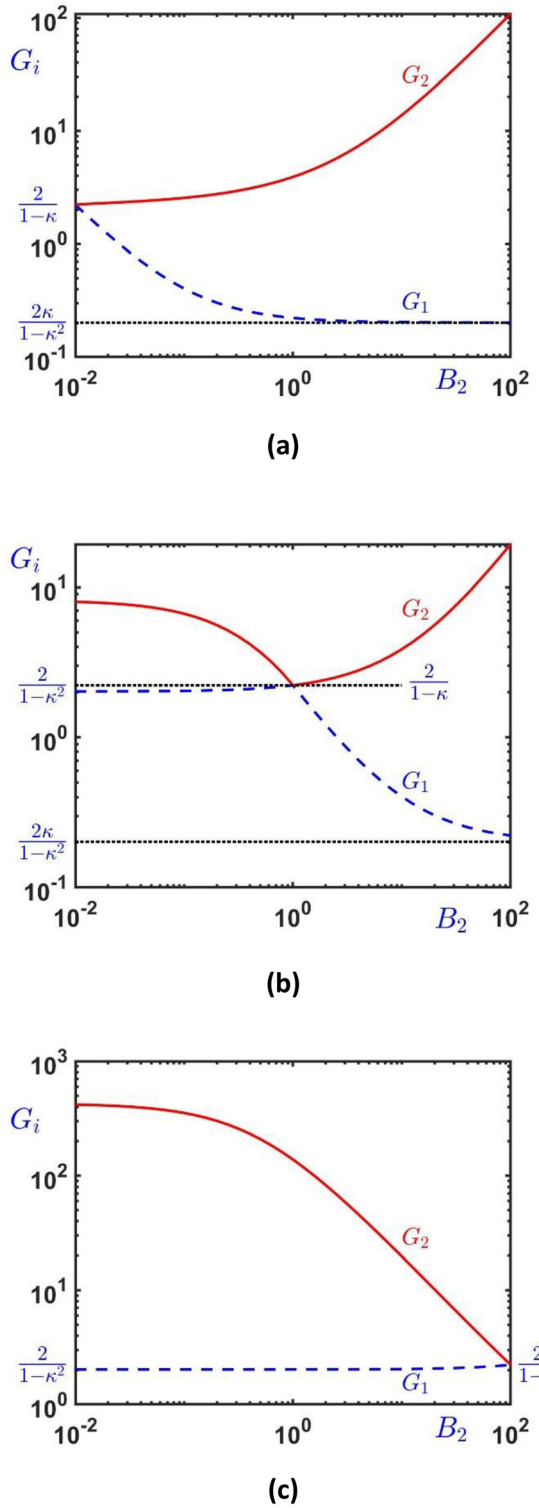

FIG. 6. Variation of the two critical pressure gradients G_1 (dashed) and G_2 (solid) with the outer slip number B_2 when $\kappa = 0.1$: (a) $B_1 = 0.01$ (weak slip); (b) $B_1 = 1$ (moderate slip); (c) $B_1 = 100$ (strong slip).

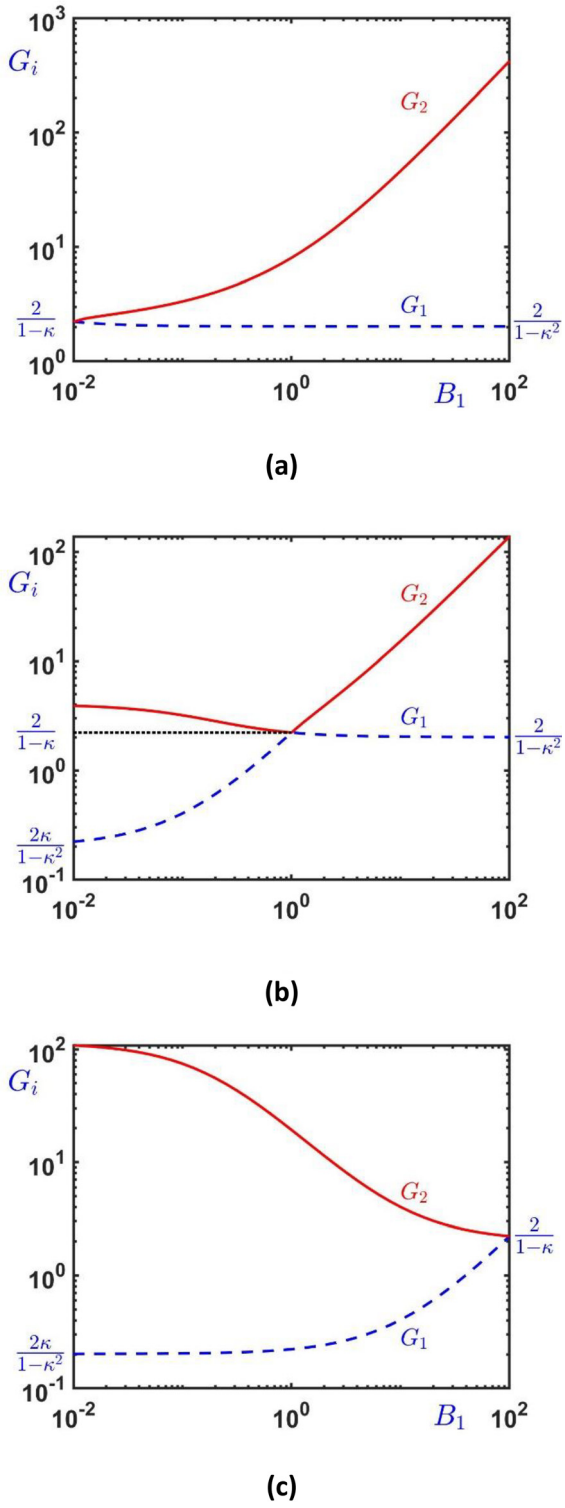

FIG. 7. Variation of the two critical pressure gradients G_1 (dashed) and G_2 (solid) with the inner slip number B_1 when $\kappa = 0.1$: (a) $B_2 = 0.01$ (weak slip); (b) $B_2 = 1$ (moderate slip); (c) $B_2 = 100$ (strong slip).

or

$$u(r) = \begin{cases} \dfrac{B_1 G}{2\kappa}(\lambda^2 - \kappa^2) + \dfrac{G}{4}\left[2\lambda^2 \ln \dfrac{r}{\kappa} - r^2 + \kappa^2 - \dfrac{4}{G}(r - \kappa)\right], \\ \qquad\qquad \kappa \le r \le \lambda, \\ \dfrac{B_2 G}{2}(1 - \lambda^2), \quad \lambda_1 \le r \le 1\,. \end{cases} \tag{60}$$

The constants λ and λ_1 are found by demanding that $\tau_{rz}(\lambda_1) = 1$ and $u_I(\lambda_1) = u_{w2}$, which yield

$$\lambda^2 = \lambda_1\left(\lambda_1 + \frac{2}{G}\right) \tag{61}$$

and

$$\frac{G}{4}\left[2\lambda^2 \ln \frac{\lambda_1}{\kappa} - \lambda_1^2 + \kappa^2 - \frac{4}{G}(\lambda_1 - \kappa)\right] + u_{w1} - u_{w2} = 0. \tag{62}$$

Combining the last equation with Eq. (39) leads to the following equation for λ_1:

$$2\lambda^2 \ln \frac{\lambda_1}{\kappa} - \lambda_1^2 + \kappa^2 - \frac{4}{G}(\lambda_1 - \kappa) + 2\left[\frac{B_1}{\kappa}(\lambda^2 - \kappa^2) - B_2(1 - \lambda^2)\right] = 0. \tag{63}$$

Once λ_1 is calculated, all other quantities of interest can be calculated, that is, λ from Eq. (61), the wall shear stresses from Eq. (28), and the velocity from Eq. (60). Since there is no region II, the volumetric flow rate is given by [see Eq. (34)]

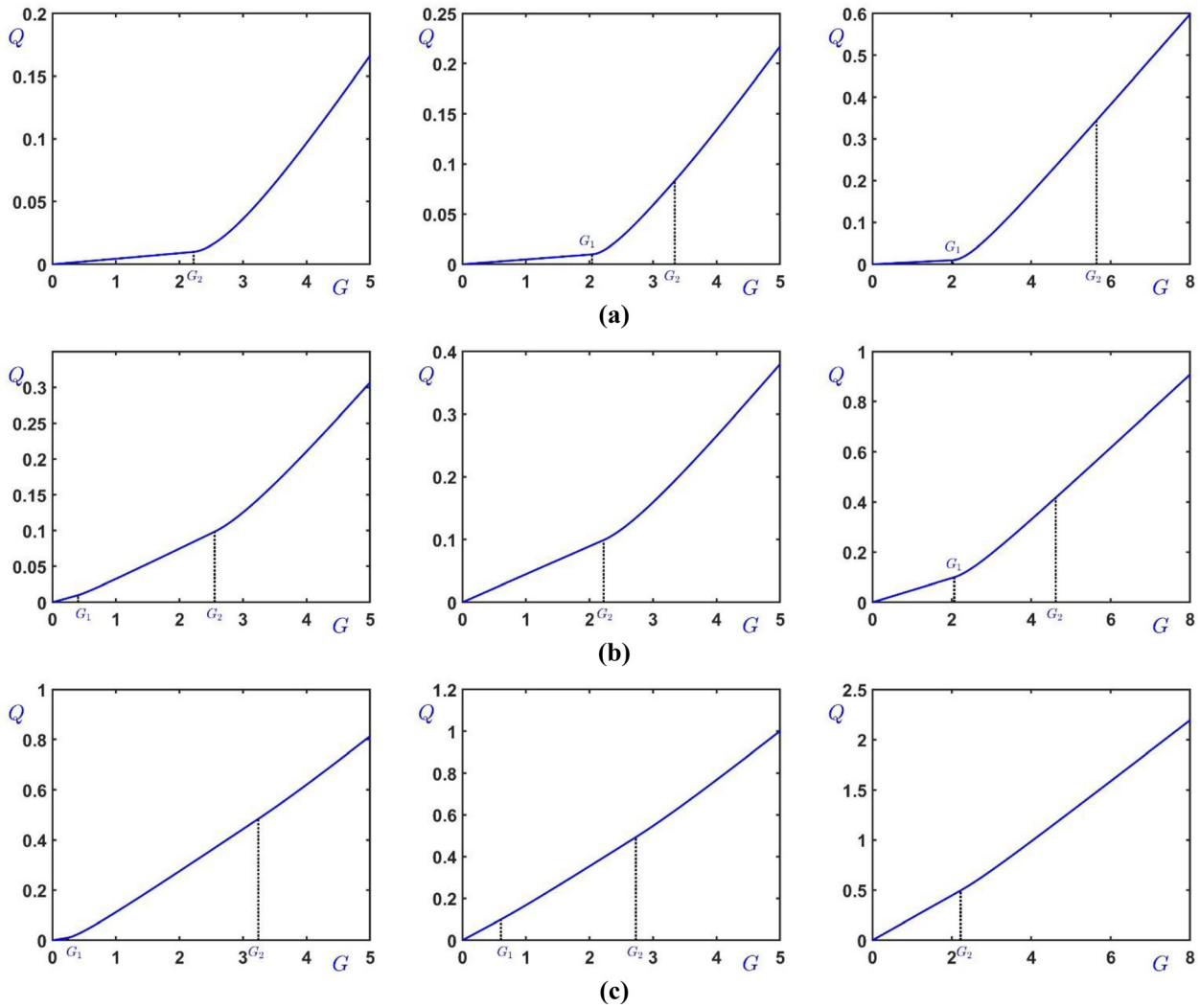

FIG. 8. Flow curves when $\kappa = 0.1$ and $B_1 = 0.01$ (weak slip, left column), 0.1 (moderate slip, middle column), and 0.5 (strong slip, right column) for various values of the outer slip number: (a) $B_2 = 0.01$; (b) $B_2 = 0.1$; (c) $B_2 = 0.5$.

$$Q = \frac{G}{2}\left[\frac{1}{4}\left(\lambda_1^4 - \kappa^4\right) + \frac{2}{3G}\left(\lambda_1^3 - \kappa^3\right) - \frac{\lambda^2}{2}\left(\lambda_1^2 - \kappa^2\right)\right] + u_{w2} - \kappa^2 u_{w1}, \tag{64}$$

which after substituting the slip velocities reads

$$Q = \frac{G}{8}\left[\lambda_1^4 - \kappa^4 + \frac{8}{3G}\left(\lambda_1^3 - \kappa^3\right) - 2\lambda^2\left(\lambda_1^2 - \kappa^2\right) + 4B_2(1-\lambda^2) - 4B_1\kappa(\lambda^2 - \kappa^2)\right]. \tag{65}$$

The critical pressure gradient G_2 corresponds to $\tau_{w2} = 1$. Combining Eqs. (28) and (61), we deduce that $\lambda_c^2 = \lambda_{1c}$, and, thus,

$$G_2 = \frac{2}{1-\lambda_c^2} = \frac{2}{1-\lambda_{1c}}. \tag{66}$$

Substituting into Eq. (63), we get the following equation for λ_{1c} :

$$2\lambda_{1c}\ln\frac{\lambda_{1c}}{\kappa} + (\lambda_{1c}-\kappa)^2 - 2(\lambda_{1c}-\kappa) + 2\left[\frac{B_1}{\kappa}\left(\lambda_{1c}-\kappa^2\right) - B_2(1-\lambda_{1c})\right] = 0. \tag{67}$$

When $B_1 = B_2 = B$, the solution of the above equation is $\lambda_{1c} = \kappa$ and the two critical pressure gradients given by Eqs. (58) and (66) coincide, $G_1 = G_2 = 2/(1-\kappa)$; that is, the semi-sliding regime is not observed. When there is no slip at the inner wall ($B_1 = 0$), the first critical pressure-gradient is

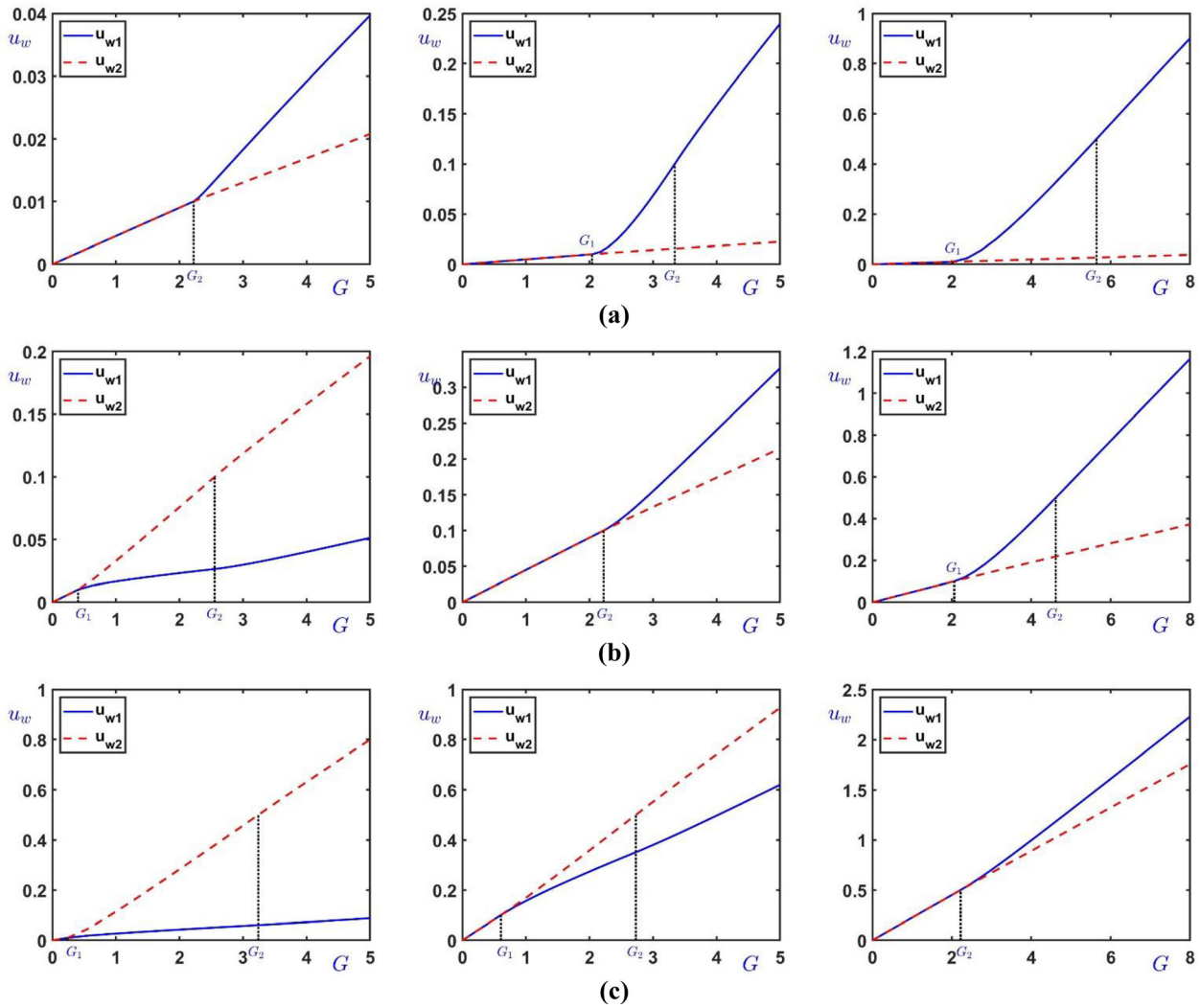

FIG. 9. Slip velocities when $\kappa = 0.1$ and $B_1 = 0.01$ (weak slip, left column), 0.1 (moderate slip, middle column), and 0.5 (strong slip, right column) for various values of the outer slip number: (a) $B_2 = 0.01$; (b) $B_2 = 0.1$; (c) $B_2 = 0.5$.

$$G_1 = \frac{2\kappa}{1-\kappa^2}. \tag{68}$$

The same value is attained asymptotically when $B_2 \to \infty$ (full slip) and B_1 is finite.

When $G \le G_1$, the material does not move and $u = 0$ (no sliding). In $[G_1, G_2]$, the velocity is given by

$$u(r) = \begin{cases} \dfrac{G}{4}\left[2\lambda^2 \ln\dfrac{r}{\kappa} - r^2 + \kappa^2 - \dfrac{4}{G}(r-\kappa)\right], & \kappa \le r \le \lambda_1, \\ \dfrac{B_2 G}{2}(1-\lambda^2), & \lambda_1 \le r \le 1, \end{cases} \tag{69}$$

and when $G > G_2$,

$$u(r) = \begin{cases} \dfrac{G}{4}\left[2\lambda^2 \ln\dfrac{r}{\kappa} - r^2 + \kappa^2 - \dfrac{4}{G}(r-\kappa)\right], & \kappa \le r \le \lambda_1, \\ \dfrac{G}{4}\left[2\lambda^2 \ln\dfrac{\lambda_1}{\kappa} - \lambda_1^2 + \kappa^2 - \dfrac{4}{G}(\lambda_1-\kappa)\right], & \lambda_1 \le r \le \lambda_2, \\ \dfrac{B_2 G}{2}(1-\lambda^2) + \dfrac{G}{4}\left[-2\lambda^2 \ln\dfrac{1}{r} + 1 - r^2 - \dfrac{4}{G}(1-r)\right], & \lambda_2 \le r \le 1. \end{cases} \tag{70}$$

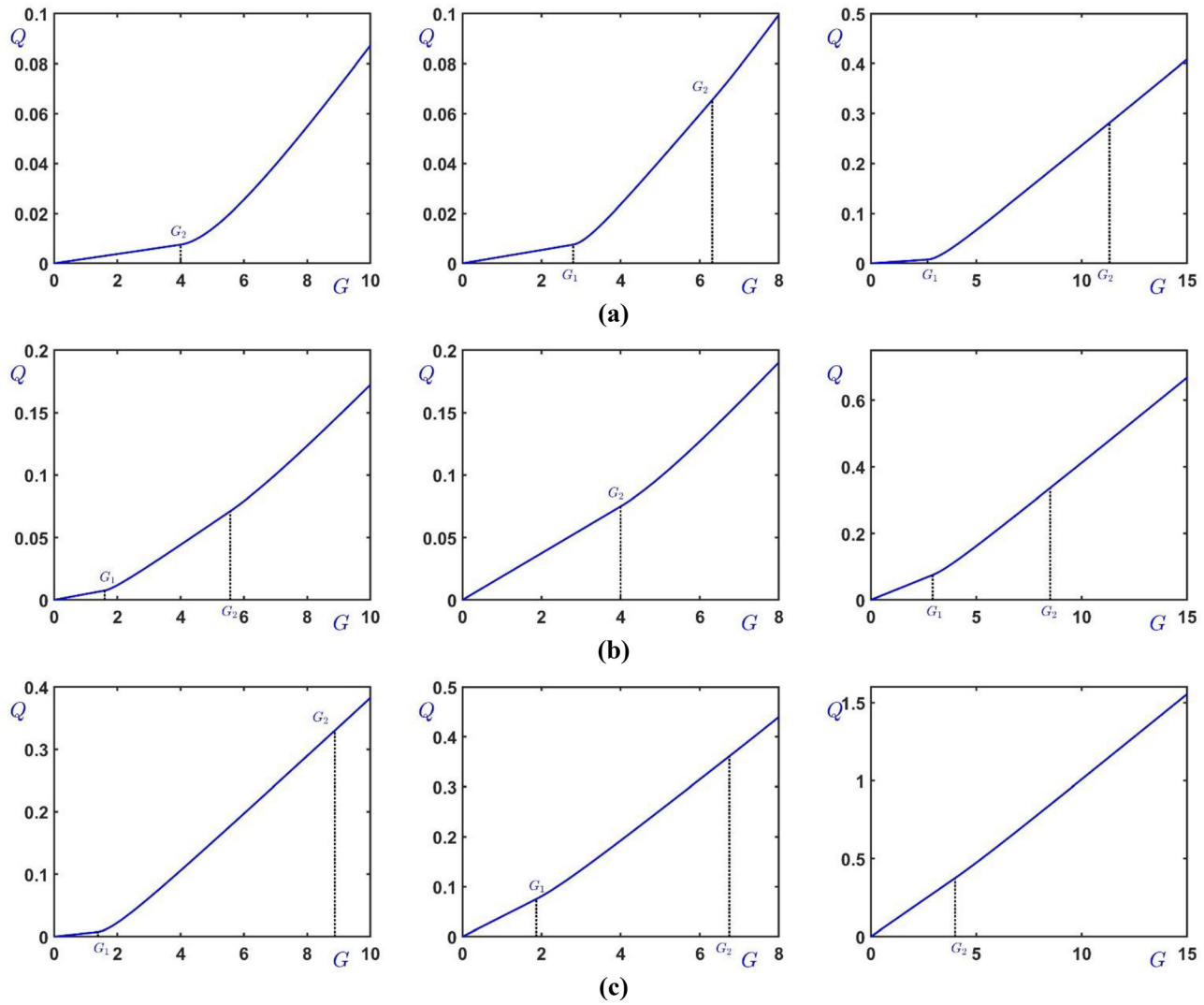

FIG. 10. Flow curves when $\kappa = 0.5$ and $B_1 = 0.01$ (weak slip, left column), 0.1 (moderate slip, middle column), and 0.5 (strong slip, right column) for various values of the outer slip number: (a) $B_2 = 0.01$; (b) $B_2 = 0.1$; (c) $B_2 = 0.5$.

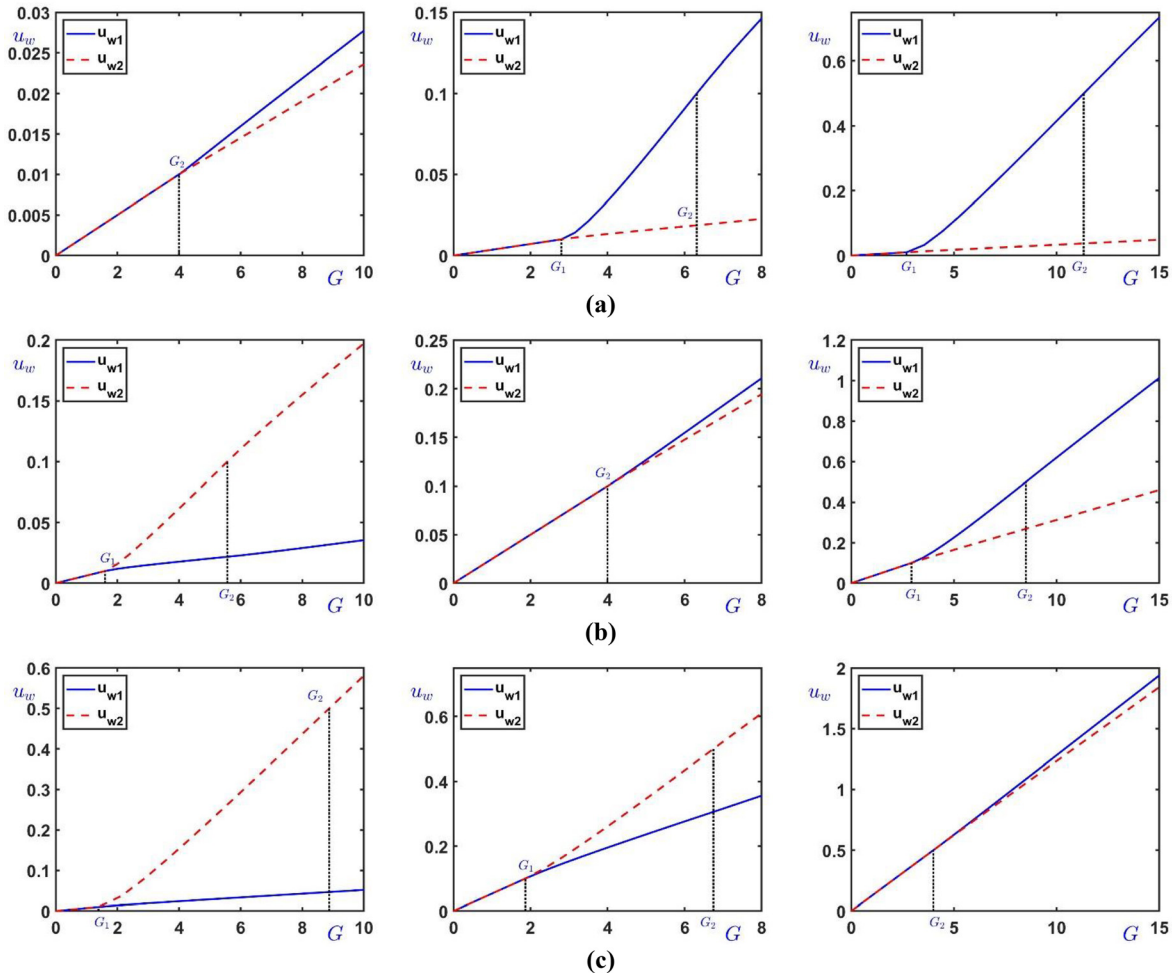

FIG. 11. Slip velocities when $\kappa = 0.5$ and $B_1 = 0.01$ (weak slip, left column), 0.1 (moderate slip, middle column), and 0.5 (strong slip, right column) for various values of the outer slip number: (a) $B_2 = 0.01$; (b) $B_2 = 0.1$; (c) $B_2 = 0.5$.

E. Stronger slip at the inner wall ($B_1 > B_2$)

The critical values G_1 and G_2 of the pressure gradient defining the semi-sliding regime when slip at the inner wall is stronger correspond to $\tau_{w2} = 1$ and $\tau_{w1} = 1$, respectively. Using Eq. (43), the following expression is obtained for G_1:

$$G_1 = \frac{2(B_1 + \kappa B_2)}{B_1(1-\kappa^2)}. \tag{71}$$

When $G_1 < G \le G_2$, the material adjacent to the inner cylinder is unyielded (λ_1 is not relevant, as there is no region I). As illustrated in Fig. 5, the velocity is given by

$$u(r) = \begin{cases} u_{w1}, & \kappa \le r \le \lambda_2, \\ u_{w2} + \dfrac{G}{4}\left[-2\lambda^2 \ln\dfrac{1}{r} - r^2 + 1 - \dfrac{4}{G}(1-r)\right], & \lambda_2 \le r \le 1, \end{cases} \tag{72}$$

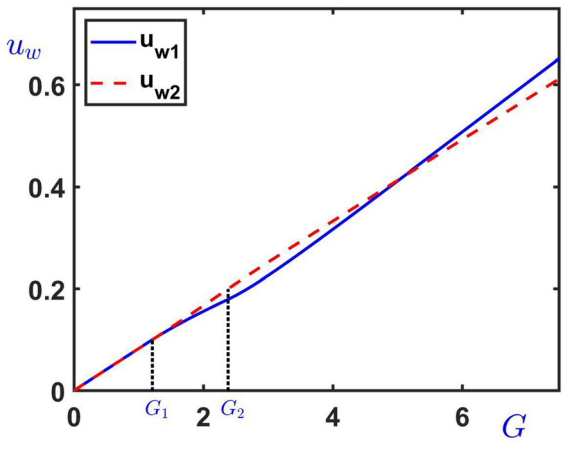

FIG. 12. The slip velocities are intersecting when slip at the outer cylinder is slightly stronger; $\kappa = 0.1$, $B_1 = 0.1$, and $B_2 = 0.2$.

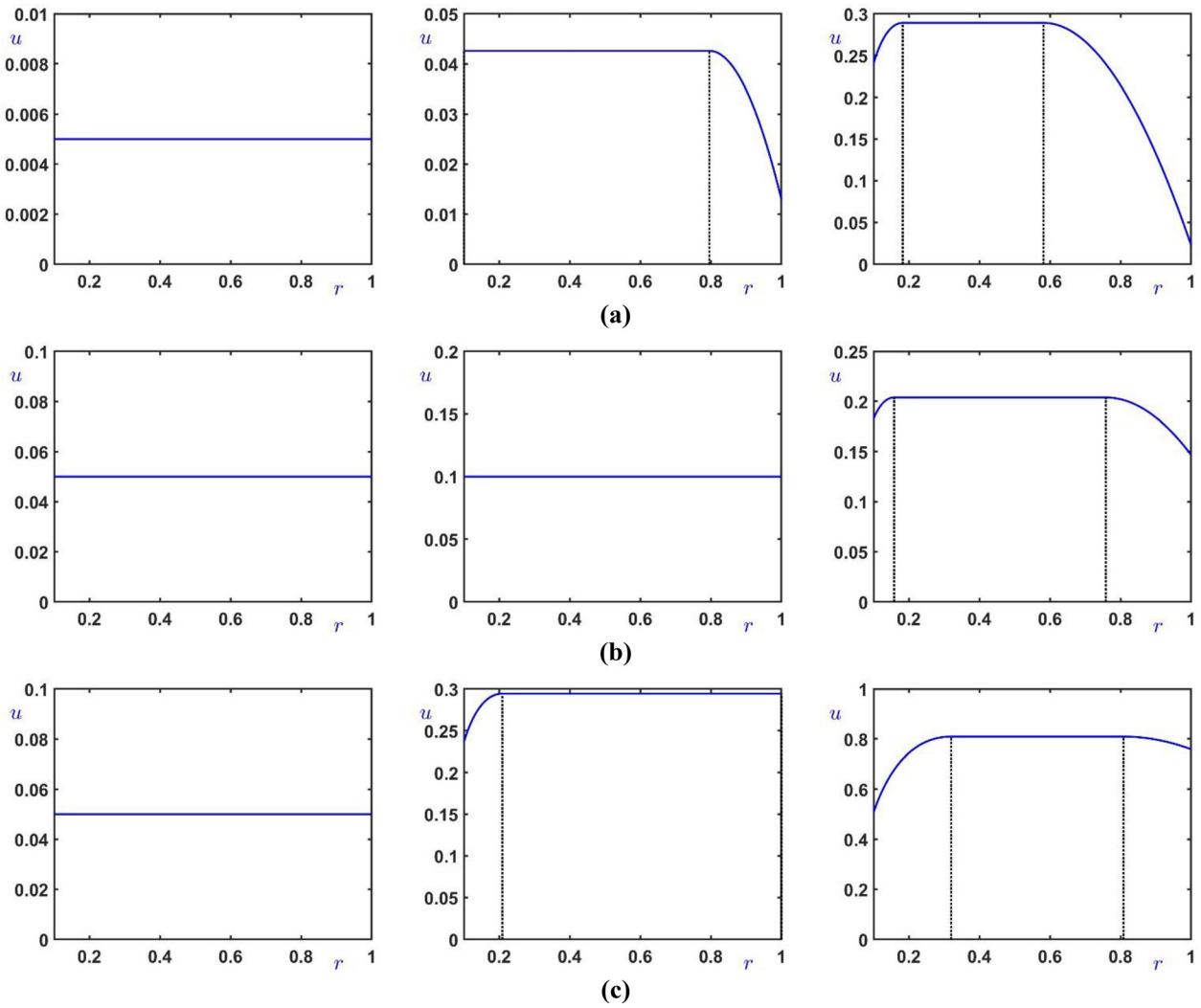

FIG. 13. Velocity profiles for $\kappa = 0.1$ at $G = G_1/2$ (sliding regime, first column), $G = (G_1 + G_2)/2$ (semi-sliding regime, middle column), and $G = 1.5G_2$ (yielding regime, right column): (a) $B_1 = 0.1$, $B_2 = 0.01$ ($G_1 = 2.0404$, $G_2 = 3.3418$); (b) $B_1 = B_2 = 0.1$ ($G_1 = G_2 = 2.2222$, no semi-sliding regime); (c) $B_1 = 0.1$, $B_2 = 0.5$ ($G_1 = 0.6061$, $G_2 = 2.7290$). The dashed lines indicate the yield radii λ_1 and λ_2.

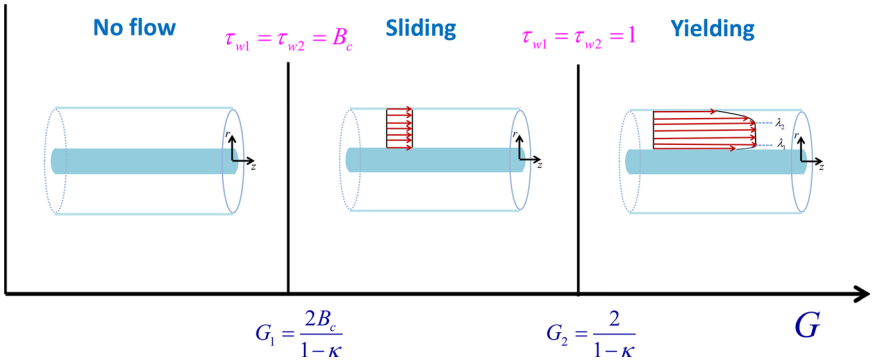

FIG. 14. Flow regimes of annular visco-plastic Poiseuille flow with wall slip with non-zero slip yield stress such that $B_c = \tau_c^*/\tau_y^* < 1$.

or

$$u(r)=\begin{cases}\dfrac{B_1G}{2\kappa}(\lambda^2-\kappa^2), & \kappa\le r\le\lambda_2,\\ \dfrac{B_2G}{2}(1-\lambda^2)+\dfrac{G}{4}\left[-2\lambda^2\ln\dfrac{1}{r}-r^2+1-\dfrac{4}{G}(1-r)\right], & \\ & \lambda_2\le r\le 1.\end{cases} \tag{73}$$

To determine λ and λ_2, we apply the conditions $-\tau_{rz}(\lambda_2)=1$ and $u_{II}(\lambda_2)=u_{w1}$, which lead to

$$\lambda^2=\lambda_2\left(\lambda_2-\frac{2}{G}\right) \tag{74}$$

and

$$\frac{G}{4}\left[2\lambda^2\ln\frac{1}{\lambda_2}-1+\lambda_2^2+\frac{4}{G}(1-\lambda_2)\right]+u_{w1}-u_{w2}=0, \tag{75}$$

which, upon substitution of the slip velocity difference [Eq. (39)], takes the form

$$2\lambda^2\ln\frac{1}{\lambda_2}-1+\lambda_2^2+\frac{4}{G}(1-\lambda_2)+2\left[\frac{B_1}{\kappa}(\lambda^2-\kappa^2)-B_2(1-\lambda^2)\right]=0. \tag{76}$$

The volumetric flow rate is given by [see Eq. (34)]

$$Q=\frac{G}{8}\left[1-\lambda_2^4-\frac{8}{3G}\left(1-\lambda_2^3\right)-2\lambda^2\left(1-\lambda_2^2\right)+4B_2(1-\lambda^2)-4B_1\kappa(\lambda^2-\kappa^2)\right]. \tag{77}$$

Setting $\tau_{w1}=1$ in Eq. (28), we find that at the critical pressure gradient G_2, $\lambda_c^2=\kappa\lambda_{2c}$, and, thus,

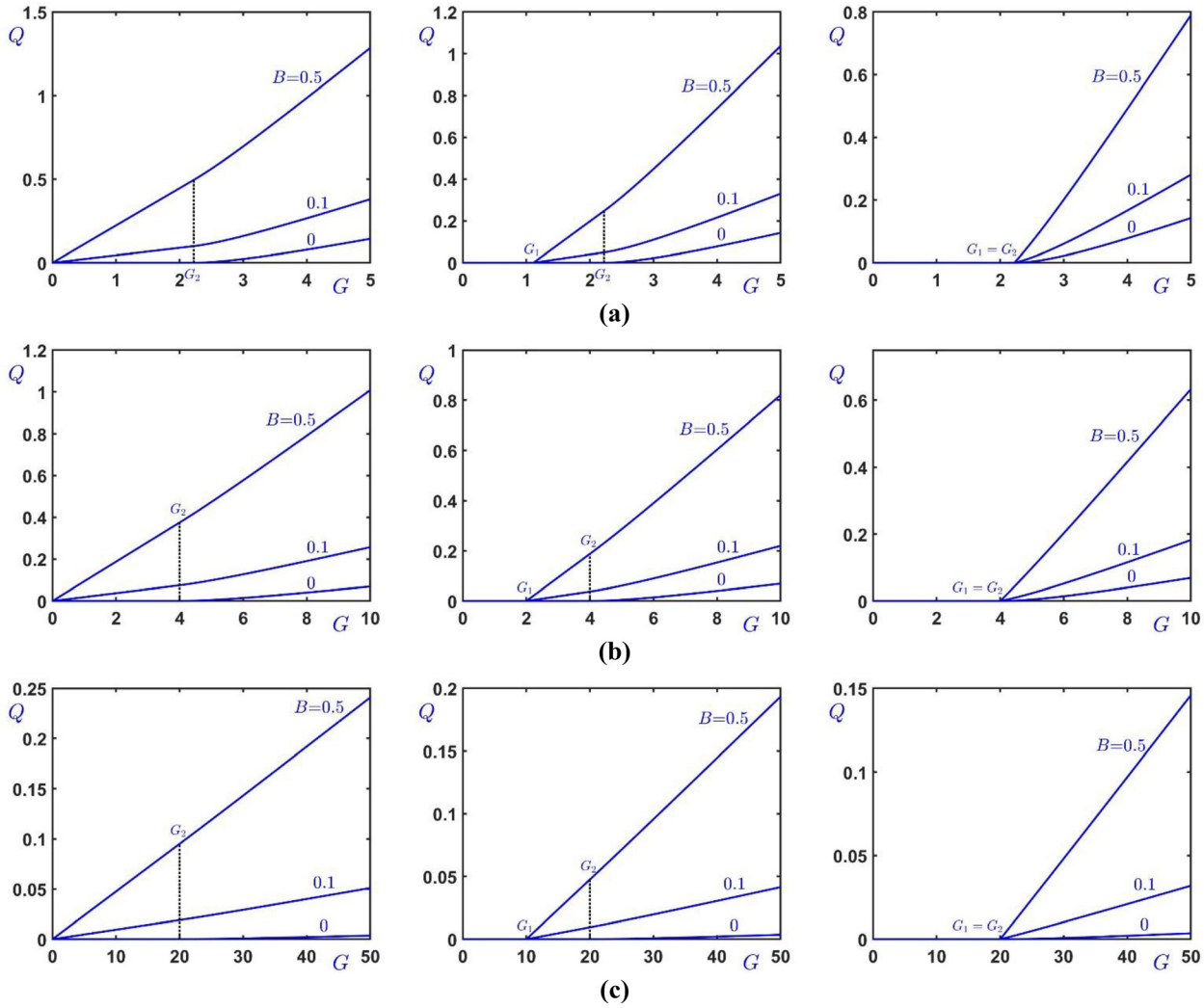

FIG. 15. Volumetric flow rates with $B_c=0$ (zero slip yield stress, left column), $B_c=0.5$ (middle column) and $B_c=1$ (the slip yield stress is the same as the yield stress, right column) and $B=0$ (no slip), 0.1, and 0.5 (very strong slip): (a) $\kappa=0.1$; (b) $\kappa=0.5$; (c) $\kappa=0.9$.

$$G_2 = \frac{2\kappa}{\lambda_c^2 - \kappa^2} = \frac{2}{\lambda_{2c} - \kappa}. \tag{78}$$

Substituting in Eq. (76), we derive the following equation for λ_{2c}:

$$2\kappa\lambda_{2c} \ln \frac{1}{\lambda_{2c}} - 1 + \lambda_{2c}^2 + 2(\lambda_{2c} - \kappa)(1 - \lambda_{2c}) + 2[B_1(\lambda_{2c} - \kappa) - B_2(1 - \kappa\lambda_{2c})] = 0. \tag{79}$$

In the special case where $B_1 = B_2 = B$, $\lambda_{2c} = 1$, $\lambda_c^2 = \kappa$, and $G_1 = G_2 = 2/(1 - \kappa)$ (the semi-sliding regime is not observed). Another interesting special case is when $B_2 = 0$, that is, when there is no slip in the outer cylinder ($u_{w2} = 0$). Equation (71) gives the first critical pressure gradient

$$G_1 = \frac{2}{1 - \kappa^2}, \tag{80}$$

below which the material does not move. The solutions in the other flow regimes are recovered by simply setting $B_2 = 0$. Finally, Eq. (80) is also attained asymptotically when B_2 is finite and $B_1 \to \infty$.

The critical pressure gradients G_1 and G_2 in all the above cases are tabulated in Table I. The variations of G_1 and G_2 with the two slip numbers B_1 and B_2 when $\kappa = 0.1$ are illustrated in Figs. 6 and 7, respectively, in the range from 10^{-2} (weak slip) to 10^2 (strong slip). One observes that G_1 increases with B_1 when this is below B_2 and vice versa. In summary, $G_1 = G_2 = 2/(1 - \kappa)$ when $B_1 = B_2$, $G_1 \to 2/(1 - \kappa^2)$ as $B_1 \to \infty$ when B_2 is finite, and $G_1 \to 2\kappa/(1 - \kappa^2)$ as $B_2 \to \infty$ when B_1 is finite.

In Fig. 8, the flow curves (i.e., the plots of the volumetric flow rate vs the pressure gradient) for $\kappa = 0.1$ and $B_1, B_2 = 0.01$, 0.1, and 0.5 are shown while the corresponding slip velocities u_{w1} and u_{w2} are plotted in Fig. 9. Figures 10 and 11 show similar results obtained with $\kappa = 0.5$. Note that if slip at the inner wall is the same or stronger that that at the

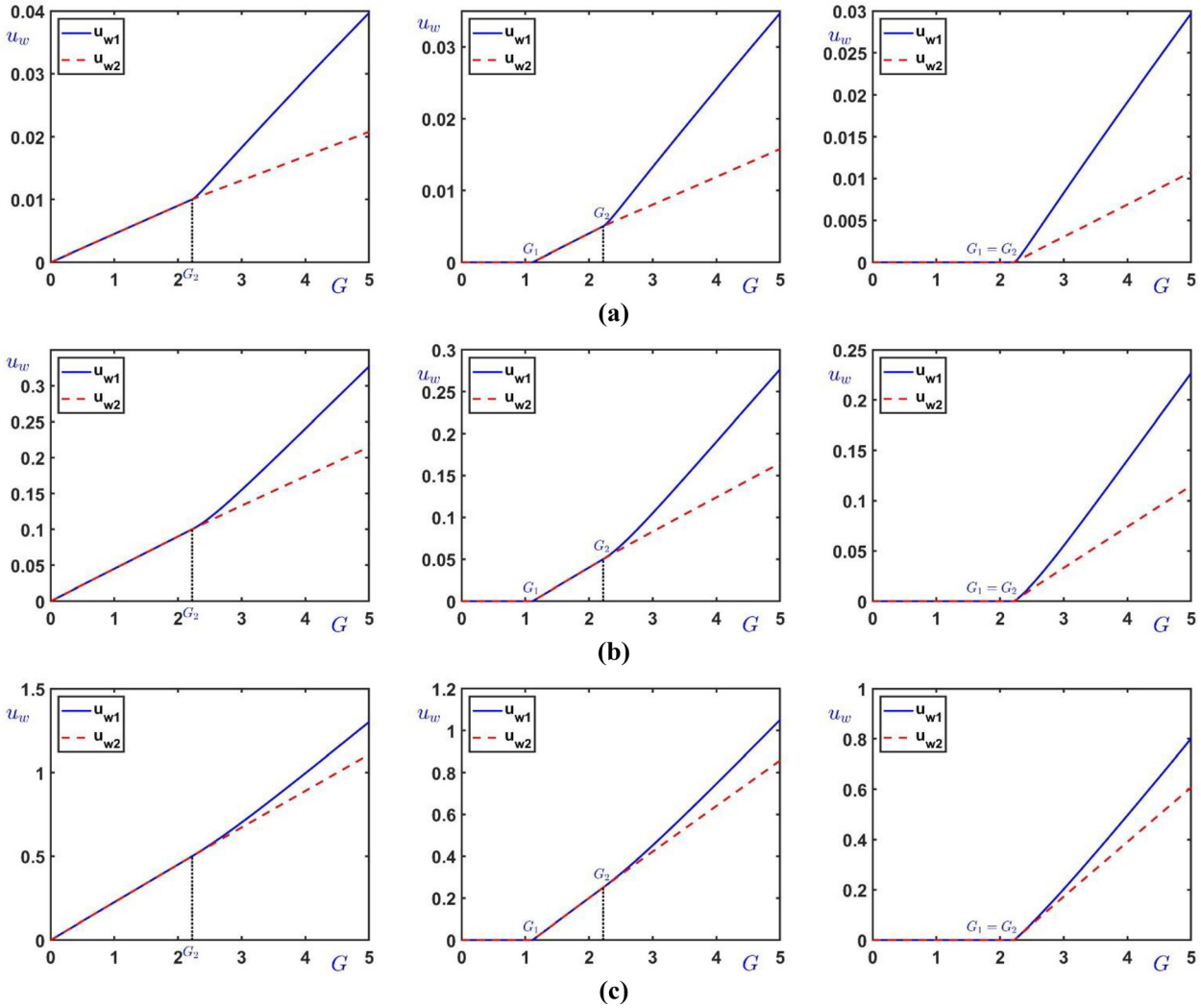

FIG. 16. Slip velocities with $\kappa = 0.1$ and $B_c = 0$ (zero slip yield stress, left column), $B_c = 0.5$ (middle column) and $B_c = 1$ (the slip yield stress is the same as the yield stress, right column): (a) $B = 0.01$ (weak slip); (b) $B = 0.1$; (c) $B = 0.5$ (very strong slip).

outer wall ($B_1 \le B_2$), then in the semi-sliding and yielding regimes, u_{w1} is bigger than u_{w2}. When slip at the outer wall is much stronger then u_{w1} is lower than u_{w2} for the entire range of pressure gradients beyond the sliding regime. If, however, slip at the outer wall is only slightly stronger, then u_{w2} is higher than u_{w1} only initially and beyond a certain pressure gradient u_{w1} grows bigger. This is illustrated in Fig. 12, where the slip velocities for $\kappa = 0.1$, $B_1 = 0.1$, and $B_2 = 0.2$ are plotted. Figure 13 shows representative velocity profiles for $\kappa = 0.1$ and $B_1, B_2 = 0.01, 0.1$, and 0.5 in all flow regimes, that is, for $G = G_1/2$ (sliding regime), $G = (G_1 + G_2)/2$ (semi-sliding regime), and $G = 1.5G_2$ (yielding regime).

By comparing those results in Figs. 9 and 11 (for $\kappa = 0.1$ and 0.5, respectively) where the same slip law applies at the two walls ($B_1 = B_2$), one observes that the two slip velocities become similar at higher values of κ, which implies that the absolute values of the wall shear stresses are also similar. For values of κ approaching unity (say for $\kappa > 0.95$), the solution approaches asymptotically the symmetric plane Poiseuille flow solution. Ortega-Avila *et al.*[12] in their experiments with an annulus of $\kappa = 0.78$ observed that the maximum difference between the slip velocities was 1.7% for the highest flow rate. They then obtained an approximate expression for the wall shear stress under the assumption that the two slip velocities are the same. Indeed, one obtains from Eqs. (28) and (29),

$$\lambda^2 \approx \kappa, \quad \lambda_1 \approx \sqrt{\frac{1}{G^2} + \kappa} - \frac{1}{G}, \quad \lambda_2 \approx \sqrt{\frac{1}{G^2} + \kappa} + \frac{1}{G}, \tag{81}$$

and

$$\tau_{w1} \approx \tau_{w2} \approx (1 - \kappa)\frac{G}{2}. \tag{82}$$

Substituting Eq. (81) into Eq. (33) results in approximate explicit expression for the velocity distribution, while Eqs. (35) and (55) become

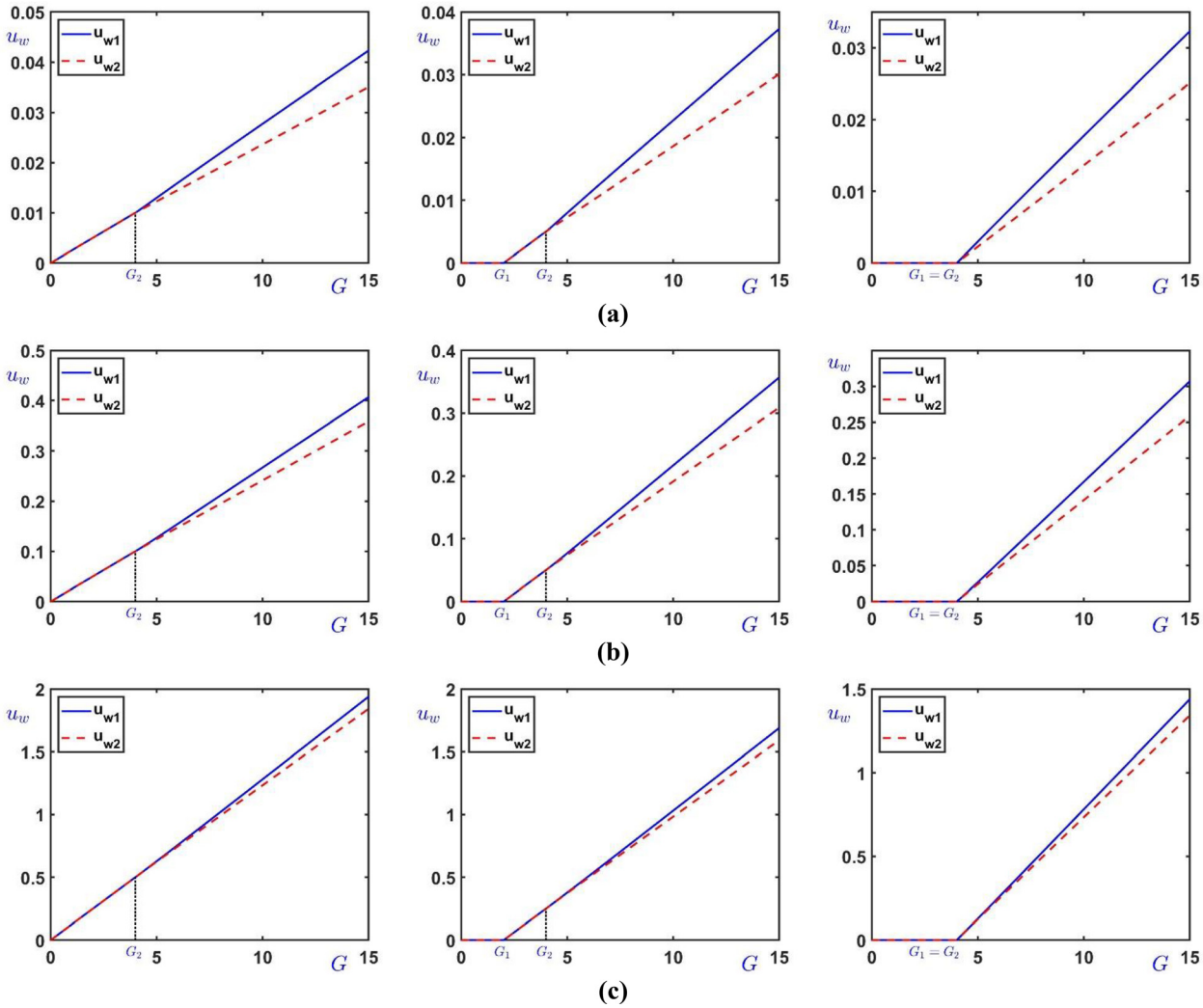

FIG. 17. Slip velocities with $\kappa = 0.5$ and $B_c = 0$ (zero slip yield stress, left column), $B_c = 0.5$ (middle column) and $B_c = 1$ (the slip yield stress is the same as the yield stress, right column): (a) $B = 0.01$ (weak slip); (b) $B = 0.1$; (c) $B = 0.5$ (very strong slip).

$$Q \approx \frac{G}{8}\left[(1-\kappa^2)^2 - \frac{8}{3G}(1+\kappa^3) + \frac{16}{3G}\left(\frac{1}{G^2}+\kappa\right)^{3/2}\right] + (1-\kappa^2)u_w \tag{83}$$

and

$$Q \approx \frac{G}{8}\left[(1-\kappa^2)^2 - \frac{8}{3G}(1+\kappa^3) + \frac{16}{3G}\left(\frac{1}{G^2}+\kappa\right)^{3/2} + 4(1-\kappa)^2(1+\kappa)B\right]. \tag{84}$$

For a given slip model, the slip velocity can be determined in terms of the approximate wall shear stress (82) and substituted in Eq. (83). Equation (84) is the resulting equation when Navier slip is applied.

IV. SLIP WITH NON-ZERO SLIP YIELD STRESS

We consider here the special case of slip law (4) when the exponent s is unity,

$$\begin{cases} u_w = 0, & \tau_w \le B_c, \\ \tau_w = B_c + \dfrac{u_w}{B}, & \tau_w > B_c, \end{cases} \tag{85}$$

where B_c is the ratio of the slip yield stress to the yield stress

$$B_c = \frac{\tau_c^*}{\tau_y^*}. \tag{86}$$

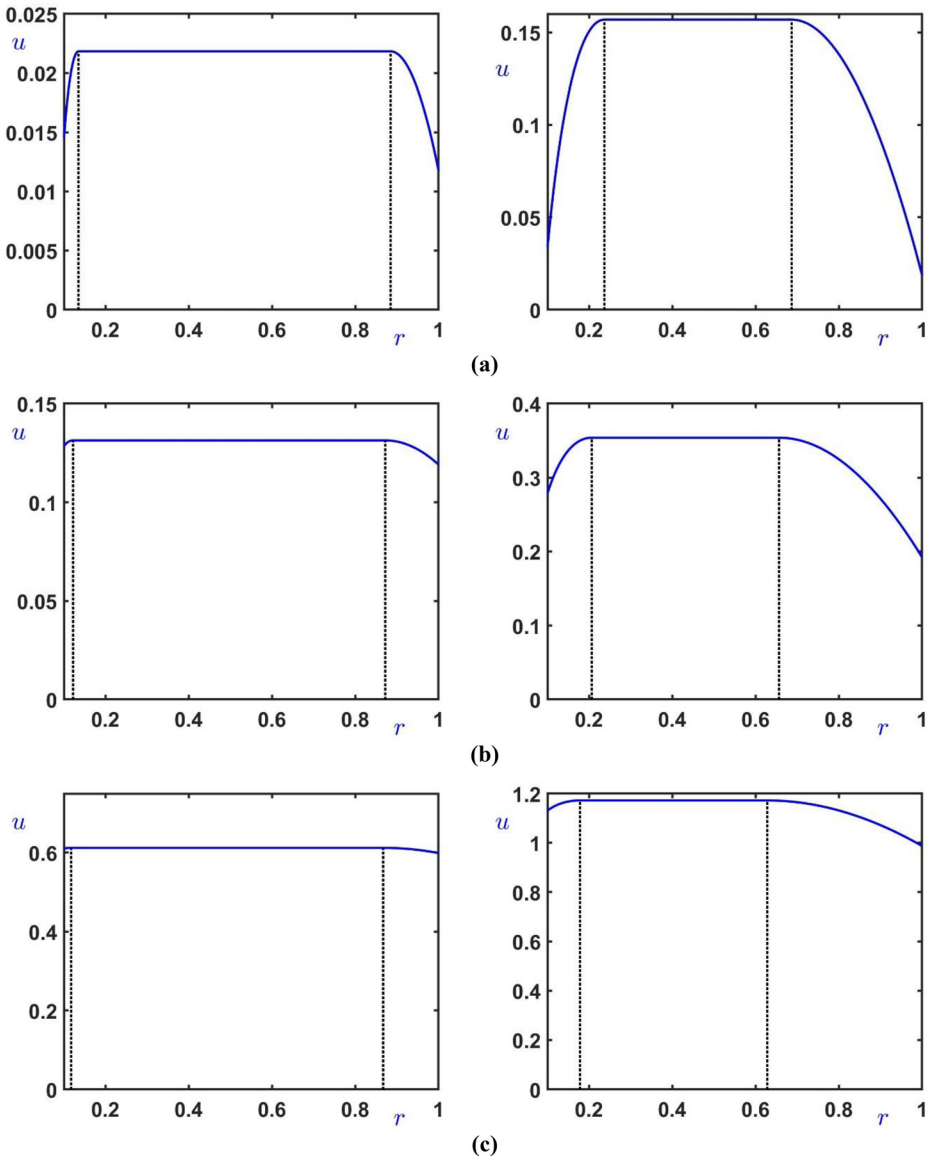

FIG. 18. Velocity profiles for $\kappa = 0.1$ and $B_c = 0$ (Navier slip) at $G = 1.2G_2$ (left column) and $G = 2G_2$ (right column): (a) $B = 0.01$ (weak slip); (b) $B = 0.1$; (c) $B = 0.5$ (very strong slip). The dashed lines indicate the yield radii λ_1 and λ_2.

As mentioned above, experimental observations on various viscoplastic materials show that the slip yield stress is lower than the yield stress,[21] and thus, $B_c \leq 1$.

When $0 < B_c < 1$, three regimes are encountered as the imposed pressure gradient is increased, that is, the no-flow, the sliding, and the yielding regimes, which are illustrated in Fig. 14. Below the critical value G_1, no slip occurs and the material remains stationary (no-flow regime). It should be noted that when $B_c = 0$ (zero slip yield stress), this regime is not encountered and Fig. 9 degenerates to Fig. 2(a) for Navier slip. Between G_1 and a second critical value G_2, the material slides as a solid (sliding regime). In this case, the wall shear stresses are equal, with $B_c < \tau_{w1} = \tau_{w2} \leq 1$. From Eq. (28), it is deduced that $\lambda^2 = \kappa$, and thus, the wall shear stresses are given by Eq. (50). Since $u_{w1} = B(\tau_{w1} - B_c)$, we get the following generalizations of Eqs. (87) and (88):

$$u = u_{w1} = u_{w2} = B\left[(1-\kappa)\frac{G}{2} - B_c\right], \quad G_1 < G \leq G_2 \tag{87}$$

and

$$Q = (1-\kappa^2)B\left[(1-\kappa)\frac{G}{2} - B_c\right], \quad G_1 < G \leq G_2. \tag{88}$$

The critical pressure gradients G_1 and G_2 are determined by demanding that $\tau_{w1} = \tau_{w2} = B_c$ and $\tau_{w1} = \tau_{w2} = 1$, respectively,

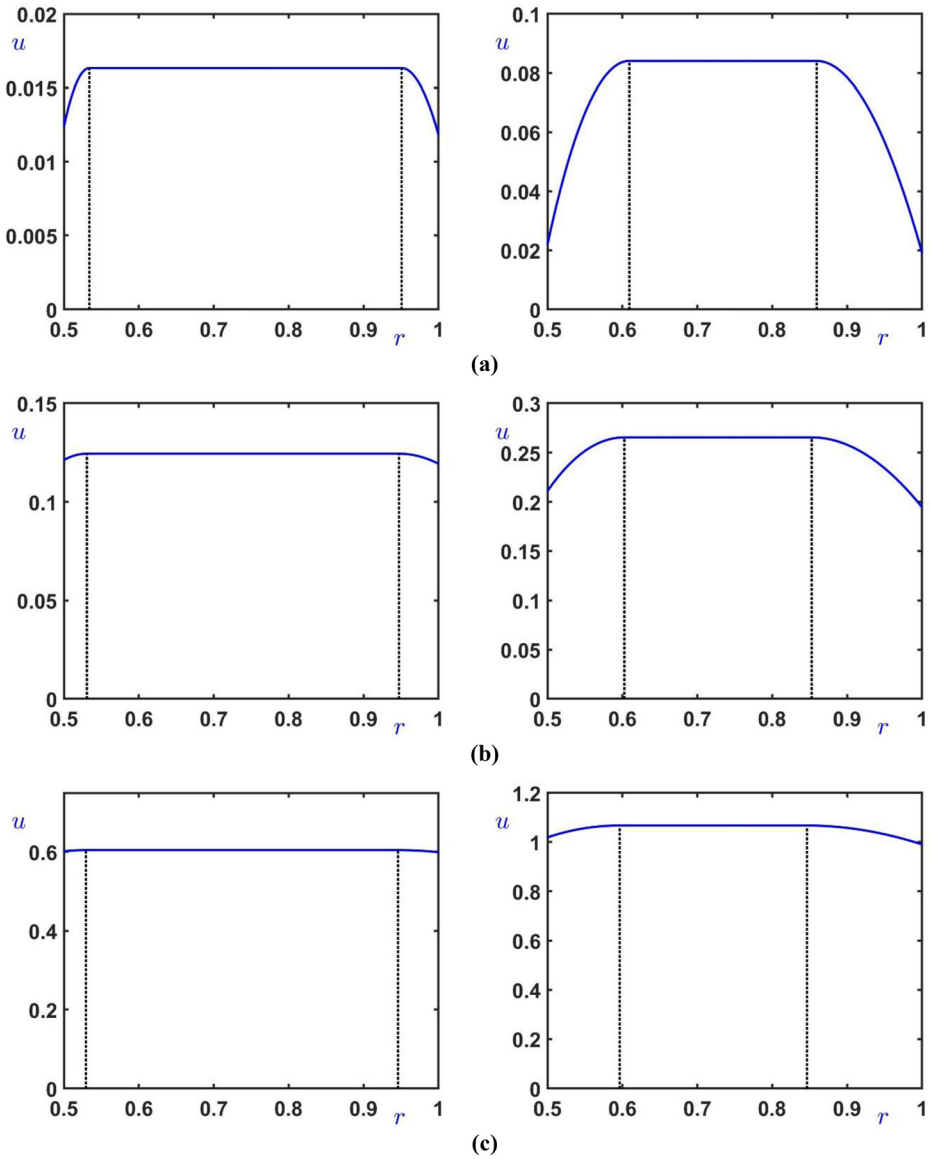

FIG. 19. Velocity profiles for $\kappa = 0.5$ and $B_c = 0$ (Navier slip) at $G = 1.2G_2$ (left column) and $G = 2G_2$ (right column): (a) $B = 0.01$ (weak slip); (b) $B = 0.1$; (c) $B = 0.5$ (very strong slip). The dashed lines indicate the yield radii λ_1 and λ_2.

$$G_1 = \frac{2B_c}{1-\kappa} \quad \text{and} \quad G_2 = \frac{2}{1-\kappa}. \tag{89}$$

When $G > G_2$, the material yields near both walls (yielding regime). It turns out that B_c does not affect the value of λ_2, which is the admissible root of Eq. (54). The two wall shear stresses are now given by Eq. (30). The slip velocities are readily obtained by means of Eq. (85),

$$u_{w1} = B(\tau_{w1} - B_c) = B\left[(\lambda^2 - \kappa^2)\frac{G}{2\kappa} - B_c\right], \quad G > G_2 \tag{90}$$

and

$$u_{w2} = B(\tau_{w2} - B_c) = B\left[(1 - \lambda^2)\frac{G}{2} - B_c\right], \quad G > G_2. \tag{91}$$

The velocity profile is given by Eq. (33). The volumetric flow is given by

$$Q = \frac{G}{8}\left\{1 - \kappa^4 - 2(1-\kappa^2)\left(\lambda_2 - \frac{2}{G}\right)\lambda_2 - \frac{8}{3G}(1+\kappa^3) + \frac{16}{3G}\left(\lambda_2 - \frac{1}{G}\right)^3 + 4B\left[1 + \kappa^3 - (1+\kappa)\left(\lambda_2 - \frac{2}{G}\right)\lambda_2 - B_c(1-\kappa^2)\frac{2}{G}\right]\right\}, \quad G > G_2, \tag{92}$$

which generalizes Eq. (55). It is clear that when $B_c = 1$, the two critical pressure gradients coincide, $G_1 = G_2 = 2/(1-\kappa)$, and the sliding regime is not observed. The slip velocities and the volumetric flow rate are obtained from Eqs. (90)–(92) by setting $B_c = 1$.

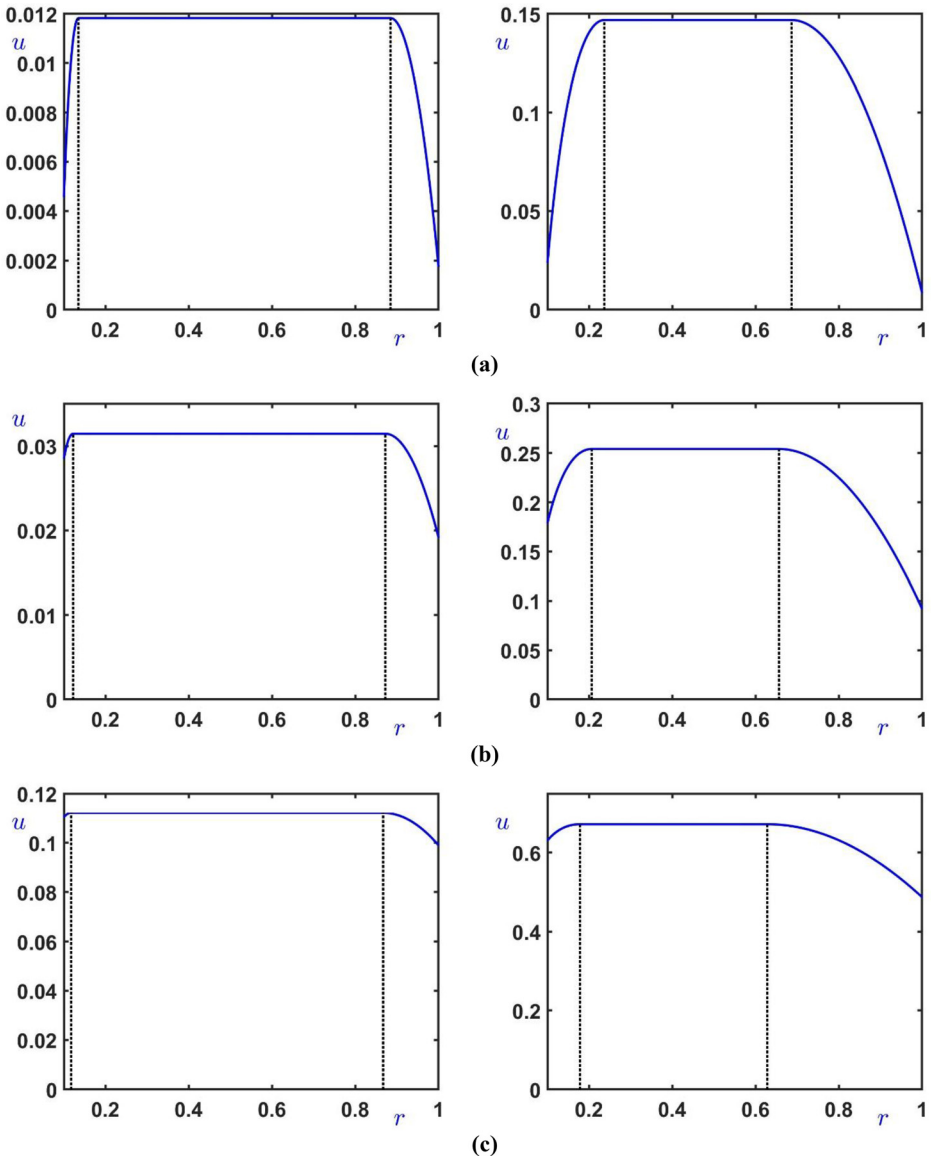

FIG. 20. Velocity profiles for $\kappa = 0.1$ and $B_c = 1$ at $G = 1.2G_2$ (left column) and $G = 2G_2$ (right column): (a) $B = 0.01$ (weak slip); (b) $B = 0.1$; (c) $B = 0.5$ (very strong slip). The dashed lines indicate the yield radii λ_1 and λ_2.

Figure 15 shows flow curves obtained for three radii ratios ($\kappa = 0.1$, 0.5, and 0.9) and three values of the slip yield stress, that is, $B_c = 0$ (zero slip yield stress), 0.5 ($\tau_c^* = \tau_y^*/2$), and 1 ($\tau_c^* = \tau_y^*$). In each case, the flow curves for $B = 0$ (no slip), 0.1 (moderate slip), and 0.5 (strong slip) are plotted. The no-flow regime is not encountered when $B_c = 0$ (Navier slip). As expected, the slope of the flow curve in the yielding regime is higher than in the sliding regime. It also increases with the slip number and decreases with the radii ratio.

The effects of the slip-yield-stress and slip numbers on the inner and outer slip velocities are illustrated in Figs. 16 and 17, for $\kappa = 0.1$ and 0.5, respectively. The slip velocities coincide in the sliding regime, while in the yielding regime, the inner slip velocity u_{w1} is always bigger than u_{w2}. The difference between the two slip velocities increases with the pressure gradient, the gap size, and the slip number B, since the velocity profile tends to become more symmetric as the gap size and slip are reduced.

Figures 18 and 19 show representative velocity profiles in the case of Navier slip ($B_c = 0$) for $\kappa = 0.1$ and 0.5, respectively, $G = 1.2G_2$ and $2G_2$, and $B = 0.01$ (weak slip), 0.1 and 0.5. These profiles become less symmetric as wall slip is enhanced, that is, as the slip number B is decreased, or as the radii ratio κ is reduced. Finally, in Figs. 20 and 21, similar results are provided for the case the slip yield stress and the yield stress are equal, that is, $B_c = 1$.

V. CONCLUSIONS

The pressure-driven flow of a Bingham plastic in an annulus has been analyzed under the assumption of wall slip along the two walls. After deriving the form of the solution in the general case in terms of

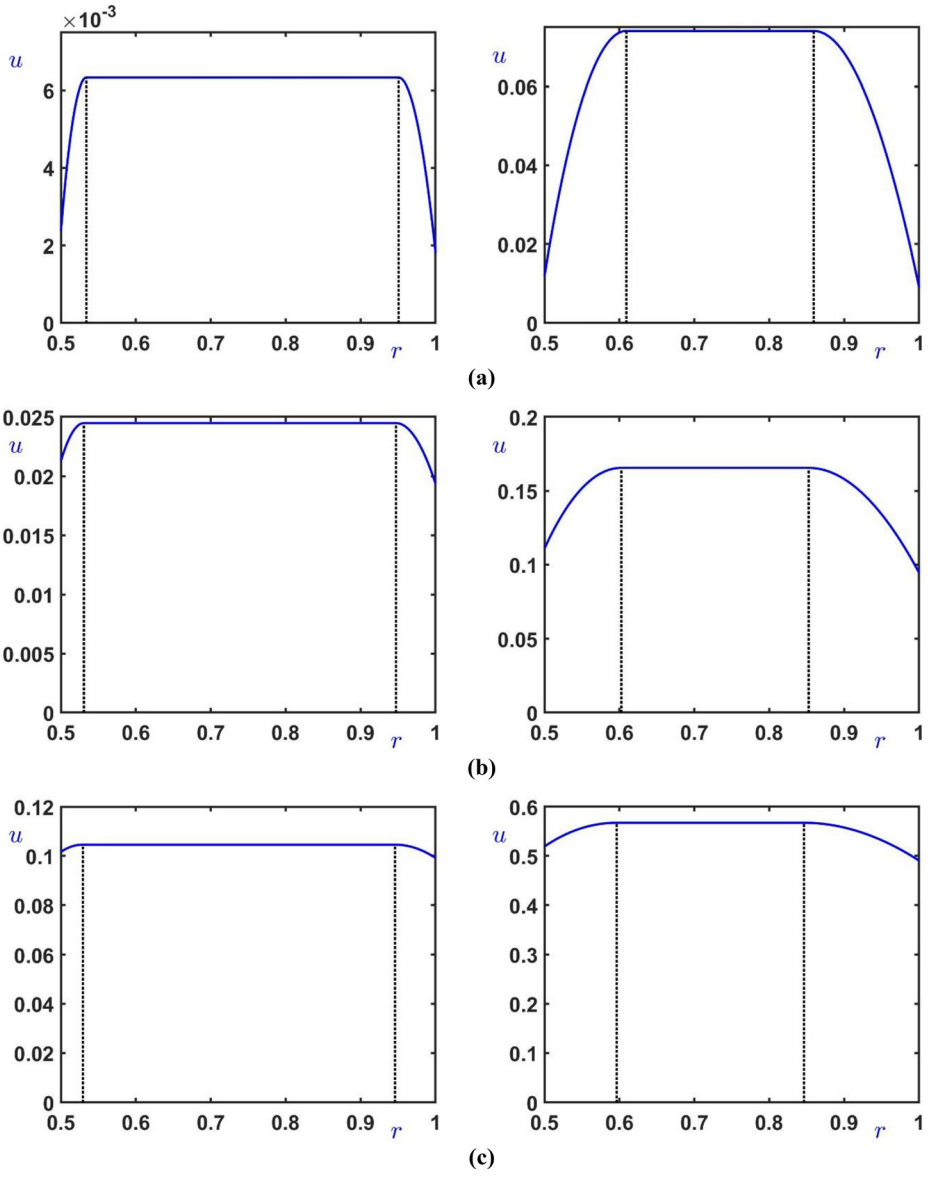

FIG. 21. Velocity profiles for $\kappa = 0.5$ and $B_c = 1$ at $G = 1.2G_2$ (left column) and $G = 2G_2$ (right column): (a) $B = 0.01$ (weak slip); (b) $B = 0.1$; (c) $B = 0.5$ (very strong slip). The dashed lines indicate the yield radii λ_1 and λ_2.

the slip velocities, two important special cases have been considered. In the first, slip yield stress is zero and different Navier slip laws apply at the two walls. In the second, the same slip law with non-zero slip yield stress is used along the two walls. In the former case, it has been demonstrated that there are three flow regimes, the sliding regime at low pressure gradients, the yielding regime at high values of the pressure gradient, and an intermediate semi-sliding regime, where the material slides unyielded along the wall where slip is stronger. The semi-sliding regime, thus, exists only when the slip coefficients at the two walls are different. The critical values of the pressure gradient, G_1 and G_2, defining the three flow regimes have been obtained, and their asymptotic values have been discussed.

In the case of non-zero slip yield stress, it has been assumed that this is less than or equal to the yields stress, that is, $B_c \leq 1$, an assumption consistent with experimental reports, and that the slip parameters at the two walls are the same ($B_1 = B_2 = B$). A no-flow regime is observed in this case, followed by the sliding and yielding regimes as the pressure gradient is increased. The effects of the slip parameters and the geometry (i.e., the radii ratio κ) have been discussed and comparisons with available solutions and experimental results in the literature have been made.

The various flow regimes discussed in this work are encountered with all yield-stress fluids, for example, a Herschel–Bulkley fluid. In fact, the solutions in the sliding regime including the corresponding critical pressure gradients are general and hold for all viscoplastic fluids, depending only on the yield stress and not on the constitutive equation. Analytical solutions for the velocity, the volumetric flow rate, and the other critical pressure gradients may be obtained only for certain values of the power-law exponent.

The results obtained employing different slip laws at the two walls and allowing the possibility of no-slip along one of them are relevant not only for processes with big annular gaps, which result in apparent slip layers of different thicknesses, but also for processes involving relatively small gaps when the wall materials of construction are different. Hence, they can guide analyses aiming at optimized tailoring of these materials and the roughness of the inner and outer walls.[12]

In this work, it has been assumed that the same slip model applies in both the sliding and yielding regimes for a given fluid/wall system. However, it is well established from various experimental studies that wall slip occurs differently in these two regimes.[12,24,35] The analysis of data on a Carbopol gel obtained in an annular geometry by Ortega-Avila *et al.*[12] yielded different power-law slip equations. More recently, Moud *et al.*[24] analyzed torsional flow data for colloidal suspensions of kaolinites and deduced that different slip models with non-zero slip-yield-stress parameters apply in the "elastic slip" (sliding) regime and the regime where the material yields and flows. In order to avoid a slip velocity jump at the transition from the sliding to the yielding regime, the slip parameters of the two models were calculated requiring that the slip velocity is a continuous function of the wall shear stress. A possible extension of the present work would, thus, be the analysis of annular Poiseuille flow of a Herschel–Bulkley fluid when different slip models apply in the two regimes. Such an analysis would be most interesting if it is combined with experimental observations.

AUTHOR DECLARATIONS

Conflict of Interest

The authors declare that they have no conflicts of interest associated with this work.

DATA AVAILABILITY

The data that support the findings of this study are available from the corresponding author upon reasonable request.

REFERENCES

[1]H. A. Barnes, "The yield stress — A review or '*πάντα ρεῖ*'- everything flows?," J. Non-Newtonian Fluid Mech. **81**, 133–178 (1999).
[2]N. J. Balmforth, I. A. Frigaard, and G. Ovarlez, "Yielding to stress: Recent developments in viscoplastic fluid mechanics," Annu. Rev. Fluid Mech. **46**, 121–146 (2014).
[3]P. Coussot, "Yield stress fluid flows: A review of experimental data," J. Non-Newtonian Fluid Mech. **211**, 31–49 (2014).
[4]A. Malkin, V. Kulichikhin, and S. Ilyin, "A modern look on yield stress fluids," Rheol. Acta **56**, 177–188 (2017).
[5]P. Coussot, "Slow flows of yield stress fluids: Yielding liquids or flowing solids," Rheol. Acta **57**, 1–14 (2018).
[6]D. Bonn, J. Paredes, M. M. Denn, L. Berthier, T. Divoux, and S. Manneville, "Yield stress materials in soft condensed matter," Rev. Mod. Phys. **89**, 035005 (2017).
[7]I. Frigaard, "Simple yield-stress fluids," Curr. Opin. Colloid Interface Sci. **43**, 80–93 (2019).
[8]E. C. Bingham, *Fluidity and Plasticity* (McGraw Hill, New York, 1922).
[9]W. Herschel and R. Bulkley, "Measurement of consistency as applied to rubber-benzene solutions," Proc., Am. Soc. Test. Mater. **26**, 621–633 (1926).
[10]M. Cloitre and R. T. Bonnecaze, "A review on wall slip in high solid dispersions," Rheol. Acta **56**, 283–305 (2017).
[11]P. Wilms, J. Wieringa, T. Blijdenstein, K. van Malssen, J. Hinrichs, and R. Kohlus, "On the difficulty of determining the apparent wall slip of highly concentrated suspensions in pressure driven flows: The accuracy of indirect methods and best practice," J. Non-Newtonian Fluid Mech. **299**, 104694 (2022).
[12]J. F. Ortega-Avila, J. Pérez-González, B. M. Marín-Santibáñez, F. Rodríguez, S. Aktas, M. Malik, and D. M. Kalyon, "Axial annular flow of a viscoplastic microgel with wall slip," J. Rheol. **60**, 503–515 (2016).
[13]E. Younes, V. Bertola, C. Castelain, and T. Burghelea, "Slippery flows of a Carbopol gel in a microchannel," Phys. Rev. Fluids **5**, 083303 (2020).
[14]C. L. M. H. Navier, "Sur les lois du mouvement des fluids," Mem. Acad. R. Sci. Inst. Fr. **6**, 389–440 (1827).
[15]S. G. Hatzikiriakos, "Wall slip of molten polymers," Progr. Polym. Sci. **37**, 624–643 (2012).
[16]E. F. Medina-Bañuelos, B. M. Marín-Santibáñez, J. Pérez-González, M. Malik, and D. M. Kalyon, "Tangential annular (Couette) flow of a viscoplastic microgel with wall slip," J. Rheol. **61**, 1007–1022 (2017).
[17]P. Wilms, J. Wieringa, T. Blijdenstein, K. van Malssen, and R. Kohlus, "Quantification of shear viscosity and wall slip velocity of highly concentrated suspensions with non-Newtonian matrices in pressure driven flows," Rheol. Acta **60**, 423–437 (2021).
[18]A. Y. Malkin and S. A. Patlazhan, "Wall slip for complex fluids–Phenomenon and its causes," Adv. Colloid Interface Sci. **257**, 42–57 (2018).
[19]J. M. Piau, "Carbopol gels: Elastoviscoplastic and slippery glasses made of individual swollen sponges: Mesoand macroscopic properties, constitutive equations and scaling laws," J. Non-Newtonian Fluid Mech. **144**, 1–29 (2007).
[20]P. Ballesta, G. Petekidis, L. Isa, W. C. K. Poon, and R. Besseling, "Wall slip and flow of concentrated hard-sphere colloidal suspensions," J. Rheol. **56**, 1005–1037 (2012).
[21]Y. Damianou, P. Panaseti, and G. C. Georgiou, "Viscoplastic Couette flow in the presence of wall slip with non-zero slip yield stress," Materials **12**(21), 3574 (2019).
[22]S. G. Hatzikiriakos, "Slip mechanisms in complex fluid flows," Soft Matter **11**, 7851–7856 (2015).
[23]M. Chaparian and O. Tammisola, "Sliding flows of yield-stress fluids," J. Fluid Mech. **911**, A17 (2021).
[24]A. A. Moud, J. Piette, M. Danesh, G. C. Georgiou, and S. G. Hatzikiriakos, "Apparent slip in colloidal suspensions," J. Rheol. **66**(1), 79–90 (2022).
[25]Y. Damianou, M. Philippou, G. Kaoullas, and G. C. Georgiou, "Cessation of viscoplastic Poiseuille flow with wall slip," J. Non-Newtonian Fluid Mech. **203**, 24–37 (2014).

[26]L. L. Ferrás, A. M. Afonso, M. A. Alves, J. M. Nóbrega, and F. T. Pinho, "Annular flow of viscoelastic fluids: Analytical and numerical solutions," J. Non-Newtonian Fluid Mech. **212**, 80–91 (2014).
[27]A. D. Fredrickson and R. B. Bird, "Non-Newtonian flow in annuli," Ind. Eng. Chem. **50**(3), 347–352 (1958).
[28]R. B. Bird, G. C. Dai, and B. J. Yarusso, "The rheology and flow of viscoplastic materials," Rev. Chem. Eng. **1**, 1–70 (1983).
[29]P. O. Brunn and B. Abu-Jdayil, "Axial annular flow of plastic fluids: Dead zones and plug-free flow," Rheol. Acta **46**, 449–454 (2007).
[30]I. Ioannou and G. C. Georgiou, "Annular pressure-driven flow of a Bingham plastic with pressure-dependent rheological parameters," Rheol. Acta **58**, 699–707 (2019).
[31]R. R. Huilgol and G. C. Georgiou, "A fast numerical scheme for the Poiseuille flow in a concentric annulus," J. Non-Newtonian Fluid Mech. **285**, 104401 (2020).
[32]M. Chatzimina, G. Georgiou, K. Housiadas, and S. G. Hatzikiriakos, "Stability of the annular Poiseuille flow of a Newtonian liquid with slip along the walls," J. Non-Newtonian Fluid Mech. **159**, 1–9 (2009).
[33]S. P. Meeker, R. T. Bonnecaze, and M. Cloitre, "Slip and flow in pastes of soft particles: Direct observation and rheology," J. Rheol. **48**, 1295–1320 (2004).
[34]R. R. Huilgol, *Fluid Mechanics of Viscoplasticity* (Springer-Verlag, Berlin, 2015).
[35]P. Yaras, D. M. Kalyon, and U. Yilmazer, "Flow instabilities in capillary flow of concentrated suspensions," Rheola. Acta **33**, 48–59 (1994).